

# Radiatively-driven natural supersymmetry at the LHC

**Howard Baer<sup>a</sup>, Vernon Barger<sup>b</sup>, Peisi Huang<sup>c,d</sup>, Dan Mickelson<sup>a</sup>, Azar Mustafayev<sup>e</sup>,  
Warintorn Sreethawong<sup>f</sup> and Xerxes Tata<sup>e</sup>**

<sup>a</sup>*Dept. of Physics and Astronomy, University of Oklahoma, Norman, OK 73019, USA*

<sup>b</sup>*Dept. of Physics, University of Wisconsin, Madison, WI 53706, USA*

<sup>c</sup>*Enrico Fermi Institute, University of Chicago, Chicago, IL 60637*

<sup>d</sup>*High Energy Physics Division, Argonne National Laboratory, Argonne, IL 60439*

<sup>e</sup>*Dept. of Physics and Astronomy, University of Hawaii, Honolulu, HI 96822, USA*

<sup>f</sup>*School of Physics, Suranaree University of Technology, Nakhon Ratchasima 30000, Thailand*

*E-mail:* baer@nhn.ou.edu, barger@pheno.wisc.edu, peisi@uchicago.edu,  
mickelso@nhn.ou.edu, azar@phys.hawaii.edu, wsreethawong@hotmail.com,  
tata@phys.hawaii.edu

**ABSTRACT:** Radiatively-driven natural supersymmetry (RNS) potentially reconciles the  $Z$  and Higgs boson masses close to  $\sim 100$  GeV with gluinos and squarks lying beyond the TeV scale. Requiring no large cancellations at the electroweak scale in constructing  $M_Z = 91.2$  GeV while maintaining a light Higgs scalar with  $m_h \simeq 125$  GeV implies a sparticle mass spectrum including light higgsinos with mass  $\sim 100 - 300$  GeV, electroweak gauginos in the  $300 - 1200$  GeV range, gluinos at  $1 - 4$  TeV and top/bottom squarks in the  $1-4$  TeV range (probably beyond LHC reach), while first/second generation matter scalars can exist in the  $5-30$  TeV range (far beyond LHC reach). We investigate several characteristic signals for RNS at LHC14. Gluino pair production yields a reach up to  $m_{\tilde{g}} \sim 1.7$  TeV for  $300 \text{ fb}^{-1}$ . Wino pair production –  $pp \rightarrow \tilde{W}_2 \tilde{Z}_4$  and  $\tilde{W}_2 \tilde{W}_2$  – leads to a unique same-sign diboson (SSdB) signature accompanied by modest jet activity from daughter higgsino decays; this signature provides the best reach up to  $m_{\tilde{g}} \sim 2.1$  TeV within this framework. Wino pair production also leads to final states with  $(WZ \rightarrow 3\ell) + E_T^{\text{miss}}$  as well as  $4\ell + E_T^{\text{miss}}$  which give confirmatory signals up to  $m_{\tilde{g}} \sim 1.4$  TeV. Directly produced light higgsinos yield a clean, soft trilepton signature (due to very low visible energy release) which can be visible, but only for a not-too-small a  $\tilde{Z}_2 - \tilde{Z}_1$  mass gap. The clean SSdB signal – as well as the distinctive mass shape of the dilepton mass distribution from  $\tilde{Z}_{2,3} \rightarrow \tilde{Z}_1 \ell\ell$  decays if this is accessible – will mark the presence of light higgsinos which are necessary for natural SUSY. While an  $e^+e^-$  collider operating with  $\sqrt{s} \sim 600$  GeV should unequivocally reveal the predicted light higgsinos, the RNS model with  $m_{1/2} \gtrsim 1$  TeV may elude all LHC14 search strategies even while maintaining a high degree of electroweak naturalness.

KEYWORDS: Supersymmetry Phenomenology, Supersymmetric Standard Model, Large Hadron Collider.

## 1. Introduction to radiative natural SUSY

The CERN LHC has gathered around  $5 \text{ fb}^{-1}$  of data at  $\sqrt{s} = 7 \text{ TeV}$  and over  $20 \text{ fb}^{-1}$  at  $\sqrt{s} = 8 \text{ TeV}$ . While this data set was sufficient for the spectacular discovery of the Higgs boson at  $m_h = 125.5 \pm 0.5 \text{ GeV}$  (ATLAS/CMS combined)[1, 2], so far there is no evidence for the production of supersymmetric (SUSY) matter. The lack of evidence for SUSY has already lead to new strong mass limits[3, 4] such as

- $m_{\tilde{g}} \gtrsim 1.7 \text{ TeV}$  for  $m_{\tilde{q}} \simeq m_{\tilde{g}}$  and
- $m_{\tilde{g}} \gtrsim 1.1 - 1.3 \text{ TeV}$  for  $m_{\tilde{q}} \gg m_{\tilde{g}}$ , depending on the final state topology,

in the context of the popular mSUGRA/CMSSM model[5]. In addition, the rather large value of  $m_h \simeq 125 \text{ GeV}$  requires highly mixed top squarks with mass typically beyond the TeV scale [6]. These TeV-scale mass limits have led many physicists to question whether weak-scale supersymmetry *naturally* accommodates the weak scale, as typified by the values of the  $W^\pm$ ,  $Z$  and  $h$  masses  $\sim 100 \text{ GeV}$ .

Specifically, these limits seemingly require increased cancellations between the various terms in the well-known expression for the  $Z$ -boson mass obtained from the minimization of the one loop MSSM Higgs potential,

$$\frac{M_Z^2}{2} = \frac{m_{H_d}^2 + \Sigma_d^d - (m_{H_u}^2 + \Sigma_u^u) \tan^2 \beta}{\tan^2 \beta - 1} - \mu^2, \quad (1.1)$$

where the  $\Sigma$ s contain 1-loop corrections to the Higgs field potential (expressions are given in the Appendix of Ref. [7]). These show that *e.g.* the  $\Sigma_u^u(\tilde{t}_{1,2})$  grow rapidly with the top-squark mass<sup>1</sup> unless model parameters are correlated in a special way as discussed below. Here we will require no large cancellations between the various contributions to  $M_Z^2$ , meaning each term on the right-hand-side of Eq. (1.1) should have a magnitude comparable to  $M_Z^2/2$ . Noting that all entries in Eq. (1.1) are defined at the weak scale, we were motivated to define the electroweak (EW) fine-tuning parameter

$$\Delta_{\text{EW}} \equiv \max_i |C_i| / (M_Z^2/2). \quad (1.2)$$

Here,  $C_{H_d} = m_{H_d}^2/(\tan^2 \beta - 1)$ ,  $C_{H_u} = -m_{H_u}^2 \tan^2 \beta/(\tan^2 \beta - 1)$  and  $C_\mu = -\mu^2$ . Also,  $C_{\Sigma_u^u(k)} = -\Sigma_u^u(k) \tan^2 \beta/(\tan^2 \beta - 1)$  and  $C_{\Sigma_d^d(k)} = \Sigma_d^d(k)/(\tan^2 \beta - 1)$ , where  $k$  labels the various loop contributions included in Eq. (1.1).

We stress that because  $\Delta_{\text{EW}}$  depends only on the weak scale, it *does not include* information about any possible high scale (HS) origin of SUSY masses and couplings, and the potentially large logarithms that could enter the right-hand-side of (1.1) at the loop-level in HS models such as mSUGRA. The effect of these logarithms is captured in the usual fine-tuning measures [8, 9, 10, 11, 12, 7] such as  $\Delta_{\text{HS}}$  or  $\Delta_{\text{BG}}$ , where the latter takes into account any correlations among parameters that may be present. In contrast,  $\Delta_{\text{EW}}$  captures the *minimal* fine-tuning that must be present. The utility of  $\Delta_{\text{EW}}$  stems from the

---

<sup>1</sup>The gluino can also not be too heavy since renormalization effects from a heavy gluino tend to make top squarks heavy in models defined at very high energy scales.

fact that  $\Delta_{\text{EW}}$  is essentially determined by the SUSY spectrum, independently of the HS dynamics that generates the spectrum. SUSY models with spectra that lead to large values of  $\Delta_{\text{EW}}$  are necessarily fine-tuned, whereas a spectrum with low values of  $\Delta_{\text{EW}}$  leaves open the possibility of finding an underlying framework where the fine-tuning is small[12, 7, 13].

In order to achieve low values of  $\Delta_{\text{EW}}$ , it is necessary that  $-m_{H_u}^2$ ,  $\mu^2$  and  $-\Sigma_u^u$  all be within a factor of a few of  $M_Z^2/2$  [14, 7]. This requires,

- the higgsino mass  $|\mu|$  to lie in the 100 – 300 GeV range for  $\Delta_{\text{EW}} \lesssim 30$ ,<sup>2</sup>
- a value of  $\sqrt{m_{H_u}^2(M_{\text{GUT}})} \sim (1.3 - 2)m_0$  so that  $m_{H_u}^2$  is driven radiatively to small negative values at the weak scale, leading to  $m_{H_u}^2(\text{weak}) \sim -M_Z^2/2$ , and
- large stop mixing from  $A_0 \sim \pm 1.6m_0$ , that soften top-squark radiative corrections whilst raising  $m_h$  to the  $\sim 125$  GeV level.

In the well-known mSUGRA/CMSSM model, the lowest value of  $\Delta_{\text{EW}}$  which is found after respecting sparticle and Higgs mass constraints is  $\sim 200$ : thus, this model would necessarily be regarded as fine-tuned[12]. In the two-extra-parameter non-universal Higgs model[16] (NUHM2),  $\Delta_{\text{EW}}$  as low as 7 – 10 can be found when  $m_{H_u}^2(\text{GUT})$ ,  $\mu$  and  $A_0$  are as stated above. In this case, the NUHM2 model may be considered as an effective theory valid up to scales  $\Lambda = M_{\text{GUT}}$  which may contain a more constrained theory, with fewer free parameters, whose correlated soft terms would yield lower  $\Delta_{\text{BG}}$  values than those found in the more general effective theory. The phenomenology of this *meta-theory* – since it is essentially determined by the weak-scale SUSY spectrum – would be much the same as that from the NUHM2 model with parameter choices which yield low values of  $\Delta_{\text{EW}}$ . A survey of the LHC collider signatures which arise from the NUHM2 model – with parameter choices which yield low values of  $\Delta_{\text{EW}}$  – is the subject of this paper.

Detailed scans over NUHM2 parameter space in Ref. [7] find that low EWFT of order  $\Delta_{\text{EW}}^{-1} \sim 3 - 15\%$  can be achieved while at the same time requiring LHC sparticle mass bounds and  $m_h \sim 123 - 127$  GeV for the following parameter choices:

- $m_0 \sim 1 - 7$  TeV,
- $m_{1/2} \sim 0.3 - 1.5$  TeV,
- $A_0 \sim \pm(1 - 2)m_0$ ,
- $\tan \beta \sim 5 - 50$ ,
- $\mu \sim 100 - 300$  GeV,

while  $m_A$  may vary over a wide range of values. This framework has been dubbed *Radiatively-driven Natural Supersymmetry* (RNS), since the required value of  $-m_{H_u}^2(\text{weak}) \sim$

---

<sup>2</sup>The connection between fine-tuning and the higgsino mass breaks down if the dominant contribution to the higgsino mass is SUSY breaking [15]. If there are no singlets that couple to the higgsinos, such a contribution would be soft. In all HS models that we are aware of, the higgsino masses have a supersymmetric origin.

$M_{\tilde{Z}}^2$  is generated radiatively via running from the GUT scale. The sparticle mass spectrum of RNS differs sharply in the top-squark sector from what has been referred to as natural supersymmetry (NS) in the literature. For phenomenologically viable RNS scenarios, we find:

- the presence of four higgsino-like states with mass  $m_{\tilde{W}_1}, m_{\tilde{Z}_{1,2}} \sim 100 - 300$  GeV and with mass gap  $m_{\tilde{Z}_2} - m_{\tilde{Z}_1} \sim 10 - 30$  GeV,
- $m_{\tilde{t}_1} \sim 1 - 2$  TeV,  $m_{\tilde{t}_2, \tilde{b}_1} \sim 2 - 4$  TeV,
- $m_{\tilde{g}} \sim 1 - 5$  TeV,
- $m_{\tilde{q}, \tilde{\ell}} \sim 5 - 10$  TeV (first/second generation sfermions).

Much higher values of first/second generation scalar masses  $m_{\tilde{q}, \tilde{\ell}} \sim 10 - 30$  TeV are allowed if non-universal generations are implemented, *i.e.*  $m_0(3) < m_0(1, 2)$ . We remark that such heavy first/second generation scalars allow for at least a partial *decoupling solution* to the SUSY flavour and  $CP$  problems. The RNS scenario retains the characteristic light higgsinos of previously studied NS models. But for RNS, the top and bottom squark masses are considerably heavier than previous NS estimates, and are probably beyond LHC reach. Also, heavier values of  $m_{\tilde{g}}$  reaching up to  $\sim 5$  TeV are allowed in RNS as compared to previous NS models.

Our goal in this paper is to assess the prospects for CERN LHC operating at  $\sqrt{s} = 14$  TeV and  $30 - 300 \text{ fb}^{-1}$  (or even higher) to discover supersymmetry within the RNS context. Previous work along this line has already been presented in Ref. [17] where it was noted that SUSY models with light higgsinos give rise to a qualitatively new signature: same-sign diboson (SSdB) production accompanied by minimal hadronic activity. This signal arises from wino pair production:  $pp \rightarrow \tilde{W}_2^\pm \tilde{Z}_4 \rightarrow (W^\pm \tilde{Z}_{1,2})(W^\pm \tilde{W}_1^\mp)$ , where the higgsinos  $\tilde{Z}_2$  and  $\tilde{W}_1$  decay into very soft hadrons or leptons owing to their small mass gaps with the LSP, which is assumed to be the lightest higgsino  $\tilde{Z}_1$ . In Ref. [17], it was shown that for higher luminosity values, the SSdB signature yields a better reach for SUSY than gluino pair searches (assuming unified gaugino masses), due to the rapidly falling  $\tilde{g}\tilde{g}$  production cross section as compared to  $\tilde{W}_2 \tilde{Z}_4$  production. In this paper, we provide a detailed treatment of a variety of different signatures expected at LHC14 for the RNS model.

Towards this end, in Sec. 2, we construct a RNS model line which contains all the generic features of RNS models, but with a variable gluino mass. In Sec. 3, we show sparticle production cross sections and branching fractions along the RNS model line. Sec. 4 examines prospects for discovering gluino pair production via signals from their cascade decays. If a signal is found, then the shape of the mass distribution of opposite sign, same flavour dileptons from  $\tilde{Z}_2 \rightarrow \tilde{Z}_1 \ell \bar{\ell}$  decays of neutralinos produced via cascade decays (or directly, see Sec. 8), characterizes models with light higgsinos, as emphasized in Ref. [8, 18, 19]. In Sec. 5, we examine aspects of the characteristic same-sign diboson signature from SUSY models with light higgsinos, previously presented in Ref. [17]. In Sec. 6, we examine prospects for LHC to detect the clean trilepton signal arising from wino

pair production followed by decay to  $WZ + E_T^{\text{miss}}$ . In Sec. 7, we examine a novel  $4\ell + E_T^{\text{miss}}$  signal from wino pair production. Sec. 8 examines the possibility of detecting directly produced higgsinos – whose decays have a very low energy release in the RNS framework – in the soft trilepton channel with low jet activity. We end in Sec. 9 with a summary of our results along with a grand overview plot.

The main findings of our work is that LHC14 with  $300 \text{ fb}^{-1}$  has the capability to discover RNS SUSY models for  $m_{\tilde{g}}$  values up to  $\sim 2 \text{ TeV}$  in the SSdB and  $\tilde{g}\tilde{g}$  channels. Since RNS models maintain low EW naturalness for  $m_{\tilde{g}}$  ranging up to  $5 \text{ TeV}$ , there remains a rather large chunk of parameter space beyond the reach of LHC14. Direct higgsino detection at next generation WIMP direct detection experiments seemingly probes the entire parameter space. However, it will likely require an  $e^+e^-$  collider operating with  $\sqrt{s} \sim 600 \text{ GeV}$  to either discover the light higgsinos predicted by RNS models with  $\Delta_{\text{EW}}^{-1} < 3\%$ , or to decisively rule these out.

## 2. A radiative natural SUSY model line

The radiative natural SUSY model automatically maintains the SUSY success stories of gauge coupling unification and radiative breaking of electroweak symmetry due to a large top quark mass. These features require the MSSM (possibly augmented by gauge singlets or additional GUT multiplets) as the effective field theory up to a scale  $\Lambda$ , which we take to be  $M_{\text{GUT}} \simeq 2 \times 10^{16} \text{ GeV}$ . The low value of  $m_{H_u}^2$  (weak) that is required to obtain small  $\Delta_{\text{EW}}$  can always be realized via RG running, once the GUT-scale value of  $m_{H_u}^2$  is decoupled from matter scalar masses. In order to implement a low value of  $|\mu| \in (100 - 300) \text{ GeV}$ , we use the 2-parameter non-universal Higgs model (NUHM2)[16], wherein weak-scale values of  $\mu$  and  $m_A$  may be used as inputs in lieu of GUT-scale values of  $m_{H_u}^2$  and  $m_{H_d}^2$ . Thus, we will adopt the NUHM2 parameter set

$$m_0, m_{1/2}, A_0, \tan\beta, \mu, m_A, \quad (2.1)$$

and also take  $m_t = 173.2 \text{ GeV}$ . For our calculations, we adopt the Isajet 7.83 [20] SUSY spectrum generator Isasugra[21].<sup>3</sup>

---

<sup>3</sup>Isasugra begins the calculation of the sparticle mass spectrum with input  $\overline{DR}$  gauge couplings and  $f_b, f_\tau$  Yukawa couplings at the scale  $Q = M_Z$  ( $f_t$  running begins at  $Q = m_t$ ) and evolves the 6 couplings up in energy to scale  $Q = M_{\text{GUT}}$  (defined as the value  $Q$  where  $g_1 = g_2$ ) using two-loop RGEs. At  $Q = M_{\text{GUT}}$ , the SSB boundary conditions are input, and the set of 26 coupled two-loop MSSM RGEs [22] are evolved back down in scale to  $Q = M_Z$ . Full two-loop MSSM RGEs are used for soft term evolution, while the gauge and Yukawa coupling evolution includes threshold effects in the one-loop beta-functions, so the gauge and Yukawa couplings transition continuously from the MSSM to SM effective theories as different mass thresholds are passed. In Isasugra, the values of SSB terms which mix are frozen out at the scale  $Q \equiv M_{\text{SUSY}} = \sqrt{m_{\tilde{t}_1} m_{\tilde{t}_2}}$ , while non-mixing SSB terms are frozen out at their own mass scale [21]. The scalar potential is minimized using the RG-improved one-loop MSSM effective potential evaluated at an optimized scale  $Q = M_{\text{SUSY}}$  which accounts for leading two-loop effects [23]. Once the tree-level sparticle mass spectrum is computed, full one-loop radiative corrections are calculated for all sparticle and Higgs boson masses, including complete one-loop weak scale threshold corrections for the top, bottom and tau masses at scale  $Q = M_{\text{SUSY}}$  [24].

NUHM2 model parameter values leading to low  $\Delta_{EW} \sim 10$  (RNS solutions) were found in Ref. [7]. We use those results to construct a RNS model line which features a variable gluino mass, via

$$\begin{aligned}
m_0 &= 5 \text{ TeV}, \\
m_{1/2} &: \text{ variable between } 0.3 - 2 \text{ TeV}, \\
A_0 &= -1.6m_0, \\
\tan\beta &= 15, \\
\mu &= 150 \text{ GeV}, \\
m_A &= 1 \text{ TeV}.
\end{aligned} \tag{2.2}$$

The variation in  $m_{1/2}$  corresponds to variation in  $m_{\tilde{g}}$  from about 0.9 TeV to  $\sim 5$  TeV.

In Fig. 1, we show the value of  $\Delta_{EW}$  along the RNS model line. We see that  $\Delta_{EW}$  begins around 11 at  $m_{1/2} \sim 300$  GeV and increases only mildly with  $m_{1/2}$ , reaching  $\Delta_{EW} \sim 20$  for  $m_{1/2}$  as high as 1000 GeV. This corresponds to EWFT of  $\sim 9\%$  at the low end of  $m_{1/2}$  and  $\sim 5\%$  at around  $m_{1/2} \sim 1$  TeV.

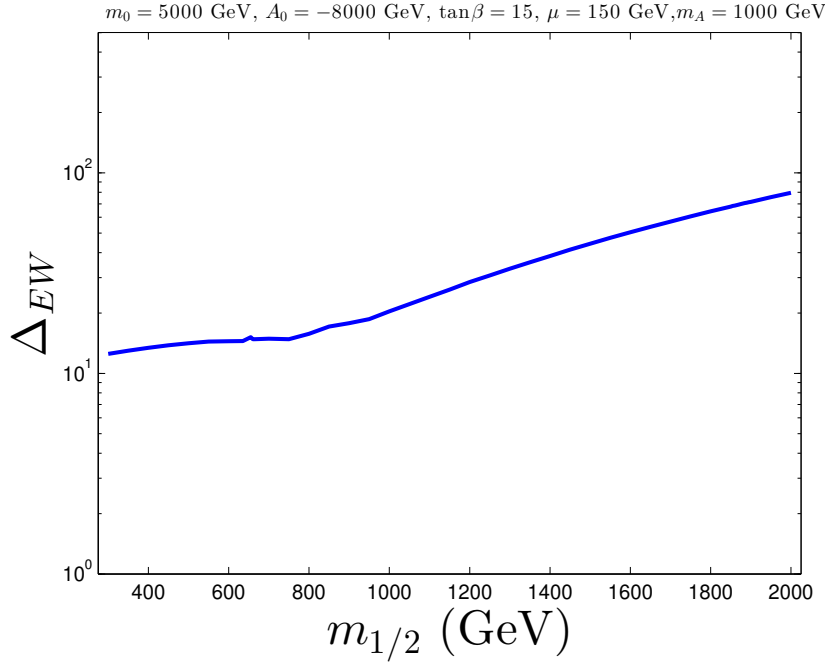


**Figure 1:** Plot of  $\Delta_{EW}$  versus  $m_{1/2}$  along the RNS model line.

In Fig. 2, we plot various sparticle masses from the RNS model line versus  $m_{1/2}$ . Along the model line, the value of  $m_h$  varies from 124.4 – 125.2 GeV, quite compatible with the recent ATLAS/CMS Higgs resonance discovery[1, 2]. Also, since  $\mu$  is fixed at 150 GeV, we obtain a spectrum of higgsino-like  $\tilde{W}_1^\pm$ ,  $\tilde{Z}_1$  and  $\tilde{Z}_2$  states with mass  $\sim 150$  GeV. However, along the model line, the mass gap  $m_{\tilde{Z}_2} - m_{\tilde{Z}_1}$  varies from 55.6 GeV for very low  $m_{1/2}$  to just under  $\sim 10$  GeV if  $m_{1/2}$  nears the values allowed by  $\Delta_{EW} \lesssim 30$ , as shown in Fig. 3.

The behaviour of light chargino/neutralino masses is easily understood since for low  $m_{1/2}$  the weak scale gaugino mass  $M_1 \simeq 136$  GeV and so the  $\tilde{Z}_1$  state is really a bino-higgsino admixture, while at  $m_{1/2} \sim 1$  TeV then  $M_1 \simeq 444$  GeV so that  $\tilde{Z}_1$  is more nearly a pure higgsino state.

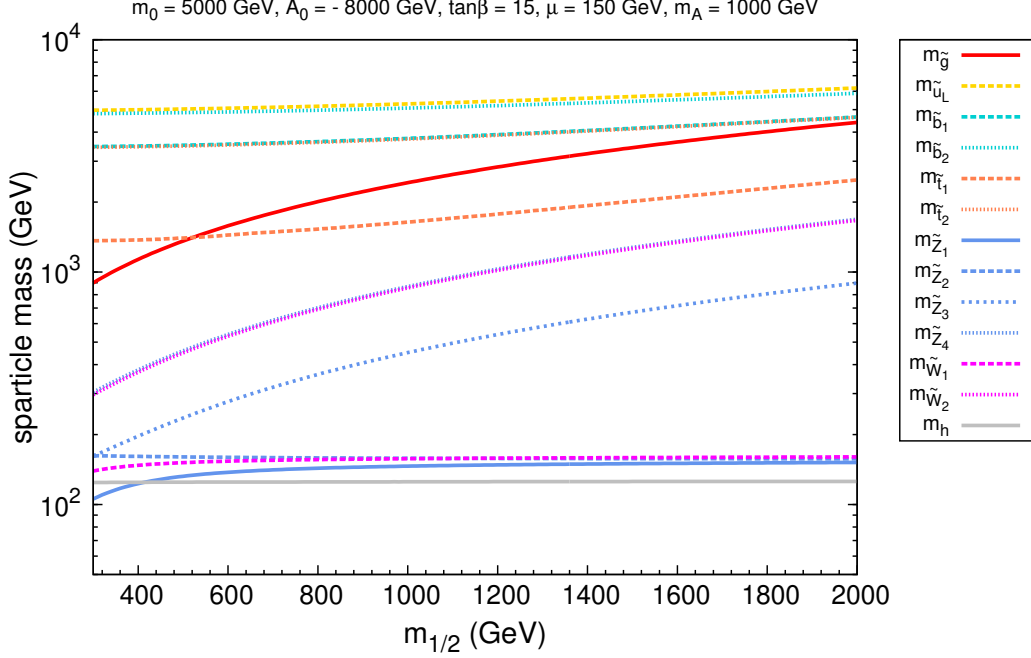


**Figure 2:** Various sparticle masses versus  $m_{1/2}$  for the RNS model line

After the higgsinos, the next lightest sparticles are the bino-like  $\tilde{Z}_3$  – whose mass varies between 160 – 900 GeV – and the wino-like  $\tilde{W}_2^\pm$  and  $\tilde{Z}_4$  states – whose masses vary between 300 – 1700 GeV – for the range of  $m_{1/2}$  shown in the figure. The solid red curve denoting  $m_{\tilde{g}}$  varies between 900 – 4500 GeV. The red-dashed  $m_{\tilde{t}_1}$  contour varies between 1360 – 2500 GeV over the  $m_{1/2}$  range shown in the figure; the line crosses the  $m_{\tilde{g}}$  curve at  $m_{1/2} \sim 520$  GeV. The first/second generation squarks and sleptons inhabit the multi-TeV range, and are far beyond the reach of LHC14.

### 3. Sparticle production and decay in RNS

In this Section, we show various particle pair production cross sections and selected sparticle branching fractions along the RNS model line in order to survey the panorama of the LHC detection possibilities.

#### 3.1 Sparticle production at LHC

In Fig. 4, we show various sparticle pair production cross sections at LHC for a)  $\sqrt{s} = 8$  TeV and b)  $\sqrt{s} = 14$  TeV versus  $m_{1/2}$  along the RNS model line. We use Prospino[25] to generate



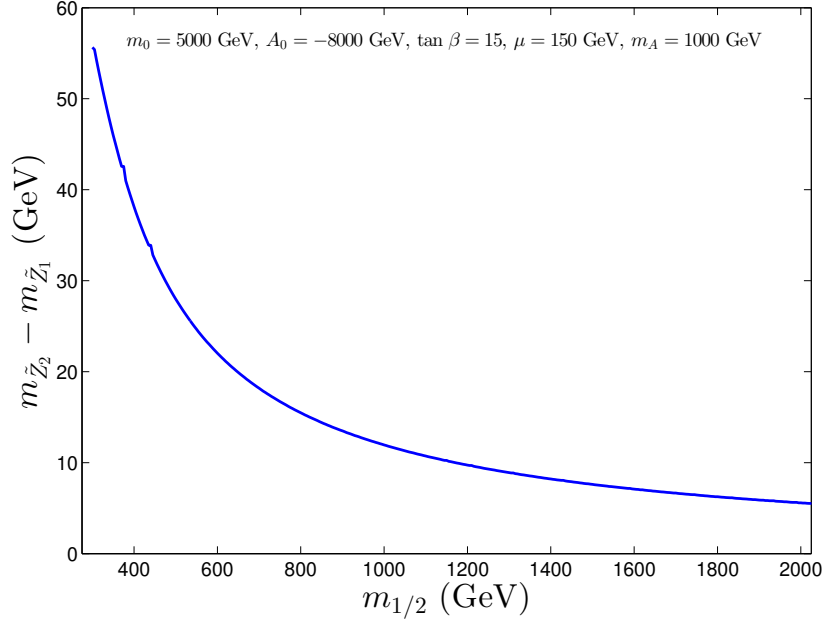


**Figure 3:** The  $m_{\tilde{Z}_2} - m_{\tilde{Z}_1}$  mass gap versus  $m_{1/2}$  along the RNS model line.

the cross sections at NLO in QCD.

From Fig. 4, we see that the four higgsino pair production reactions –  $pp \rightarrow \tilde{W}_1^\pm \tilde{Z}_1$ ,  $\tilde{W}_1^\pm \tilde{Z}_2$ ,  $\tilde{W}_1^+ \tilde{W}_1^-$  and  $\tilde{Z}_1 \tilde{Z}_2$  – all occur at comparable rates of  $\sim 500$  fb at LHC8 and of  $\sim 1000$  fb at LHC14. These cross sections are nearly flat with increasing  $m_{1/2}$  since they mainly depend on  $\mu$  which is fixed at 150 GeV along the model line.

The gluino pair production cross section –  $\sigma(pp \rightarrow \tilde{g}\tilde{g}X)$  – is denoted by the red curve with pluses. (As a guide, we note that  $m_{\tilde{g}} \simeq 2.6m_{1/2}$ .) While the  $\tilde{g}\tilde{g}$  production cross section is large at  $m_{1/2} \sim 300$  GeV (corresponding to  $m_{\tilde{g}} \sim 900$  GeV), it drops off rapidly with increasing values of  $m_{1/2}$ : it is likely to be inconsequential for even LHC14 searches for the upper range of  $m_{1/2} \gtrsim 1$  TeV unless extremely high integrated luminosities are attained.

Also of importance are the gaugino pair production reactions: wino pair production  $pp \rightarrow \tilde{W}_2^\pm \tilde{Z}_4$  and  $\tilde{W}_2^+ \tilde{W}_2^-$ , and also  $\tilde{W}_1^\pm \tilde{Z}_3$  which proceeds via the higgsino component of the bino-like  $\tilde{Z}_3$ . Wino pair production can be large due to the large  $SU(2)$  triplet gauge coupling. The cross section for this drops off much less sharply than that for  $\tilde{g}\tilde{g}$  production since the wino masses are much smaller than the gluino mass. The cross section for  $\tilde{W}_1 \tilde{Z}_3$  production falls off faster than the wino production cross section because the higgsino content of  $\tilde{Z}_3$  drops off with increasing  $m_{1/2}$ . We will see below that these reactions constitute the largest *observable* SUSY cross sections over most of the range of  $m_{1/2}$ .

For comparison, we also show cross sections for the pair production of top squarks, the lightest sfermions in RNS. The tiny  $\tilde{t}_1 \tilde{t}_1$  production cross section at  $\sqrt{s} = 8$  TeV precludes any possibility of stop detection at LHC8. Since for RNS models  $m_{\tilde{t}_1}$  lies within

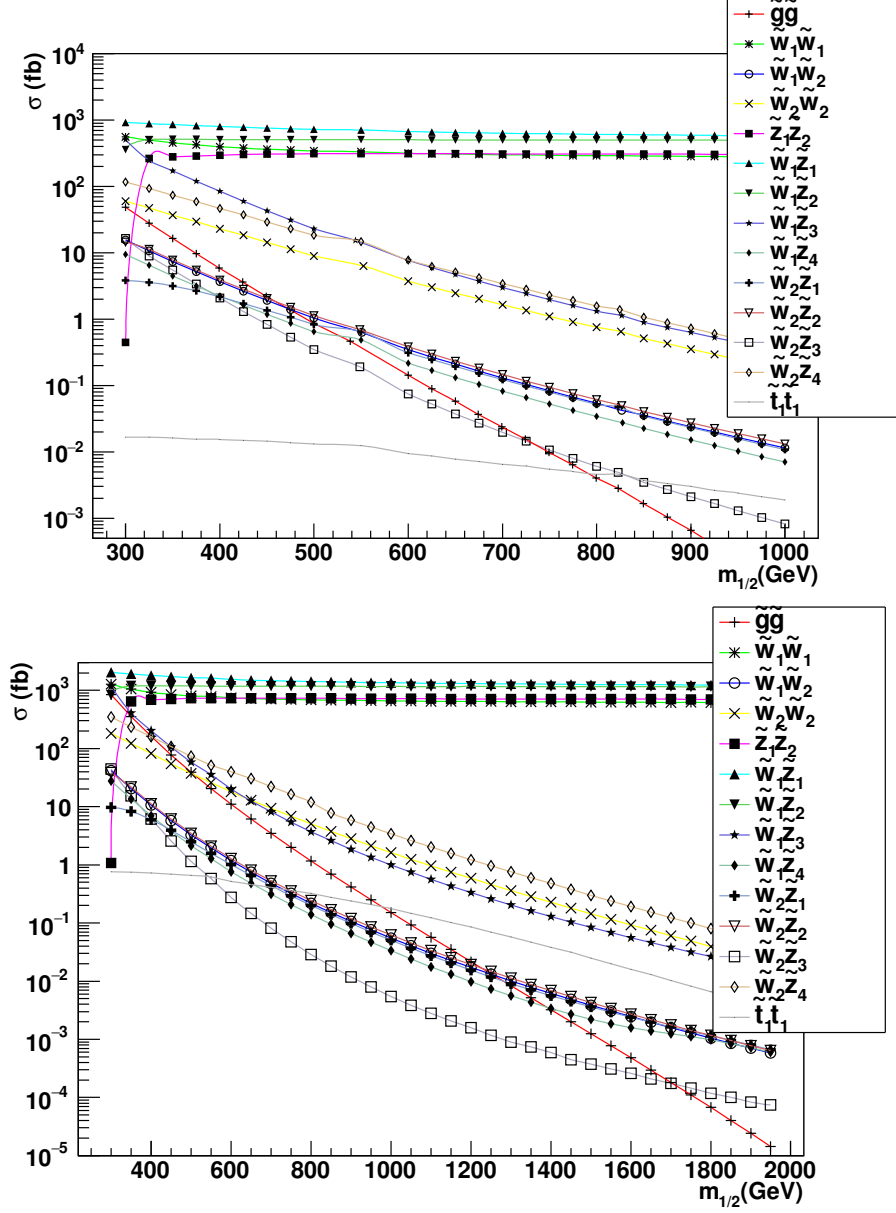


**Figure 4:** Plot of various NLO sparticle pair production cross sections versus  $m_{1/2}$  along the RNS model line for  $pp$  collisions at a)  $\sqrt{s} = 8$  TeV and b)  $\sqrt{s} = 14$  TeV.

the 1 – 2 TeV range (and  $m_{\tilde{t}_{1,2}, \tilde{b}_1}$  lies within 2 – 4 TeV) over the range where the fine-tuning is better than 3%, it is clear that their detectability at even high luminosity upgrades of LHC14 will be very difficult, and certainly not extend over the entire allowed mass range [26, 27, 28]. The top/bottom squark mass range in radiatively-driven natural SUSY differs sharply from earlier versions of natural SUSY[8, 9, 10] where third generation squarks with  $m_{\tilde{t}_{1,2}, \tilde{b}_1} \lesssim 600$  GeV are to be expected. Such light third generation squarks have difficulty generating a large enough radiative correction to allow for  $m_h \sim 125$  GeV, they lead to anomalous contributions to  $b \rightarrow s\gamma$  decay, and they likely should have already been seen

in LHC8 top squark search analyses.

In Fig. 5, we show selected electroweak-ino cross sections versus  $\mu$  for  $m_{1/2} = 750$  GeV along the RNS model line for LHC14. Here we see that  $\widetilde{W}_1\widetilde{Z}_2$ ,  $\widetilde{Z}_1\widetilde{Z}_2$  and  $\widetilde{W}_1^+\widetilde{W}_1^-$  production are all comparable and as high as  $\sim 5000$  fb at  $\mu \sim 100$  GeV. They drop to the vicinity of  $\sim 10^2$  fb at  $\mu \sim 300$  GeV. It is conceivable that a monojet search for  $pp \rightarrow \widetilde{Z}_1\widetilde{Z}_1$  production including initial state radiation of a hard gluon could reveal higgsino-like dark matter production at LHC[29]. The cross section for this reaction (and also for  $\widetilde{Z}_2\widetilde{Z}_2$  pair production) is several orders of magnitude below the other cross sections because the coupling of identical higgsino-like neutralinos to  $Z$  is dynamically suppressed, and so seems much more challenging to detect. However, this hard monojet signal may receive significant contributions from  $\widetilde{W}_1^\pm\widetilde{W}_1^\mp$ ,  $\widetilde{Z}_1\widetilde{Z}_2$  and  $\widetilde{W}_1^\pm\widetilde{Z}_2$  production processes which have much larger cross sections since the daughters from  $\widetilde{W}_1$  and  $\widetilde{Z}_2$  decays are expected to be soft at least for higher  $m_{1/2}$  values.

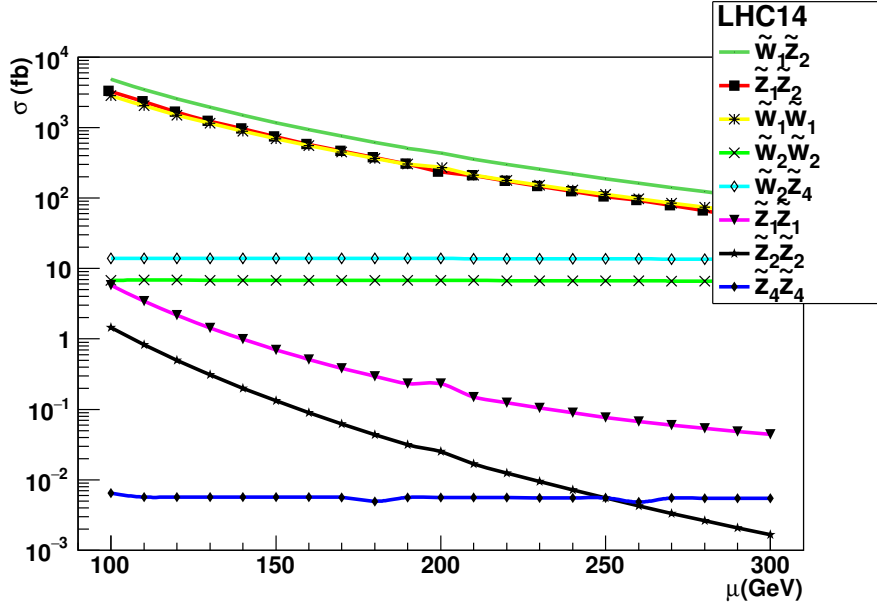


**Figure 5:** Plot of various NLO electroweak-ino pair production cross sections versus  $\mu$  for the RNS model line with  $m_{1/2} = 750$  GeV for  $pp$  collisions at 14 TeV.

### 3.2 Sparticle branching fractions

In Fig. 6, we show various sparticle branching fractions for sparticles most accessible at the LHC, *i.e.* a)  $\tilde{g}$ , b)  $\tilde{t}_1$ , c)  $\tilde{Z}_2$ , d)  $\tilde{Z}_3$ , e)  $\tilde{Z}_4$ , and f)  $\widetilde{W}_2$ . From frame a), we see that for the lower portion of  $m_{1/2}$  corresponding to  $m_{\tilde{g}} \lesssim 1.8$  TeV, the gluino decays via 3-body modes into  $t\bar{b}\widetilde{W}_1$  and  $t\bar{t}\widetilde{Z}_{1,2,3}$  states. For heavier  $m_{\tilde{g}} \gtrsim 1.8$  TeV, the 2-body modes  $\tilde{g} \rightarrow t\bar{t}_1$  open up and dominate the decays. Thus, we expect the gluino pair production events to be rich in  $b$ -jet activity[30, 31]. In the case where  $\tilde{g} \rightarrow t\bar{t}_1$ , it is important to know how  $\tilde{t}_1$  decays. This is shown in frame b). For the very lowest  $m_{1/2}$  values, the  $\tilde{t}_1 \rightarrow t\tilde{g}$  decay

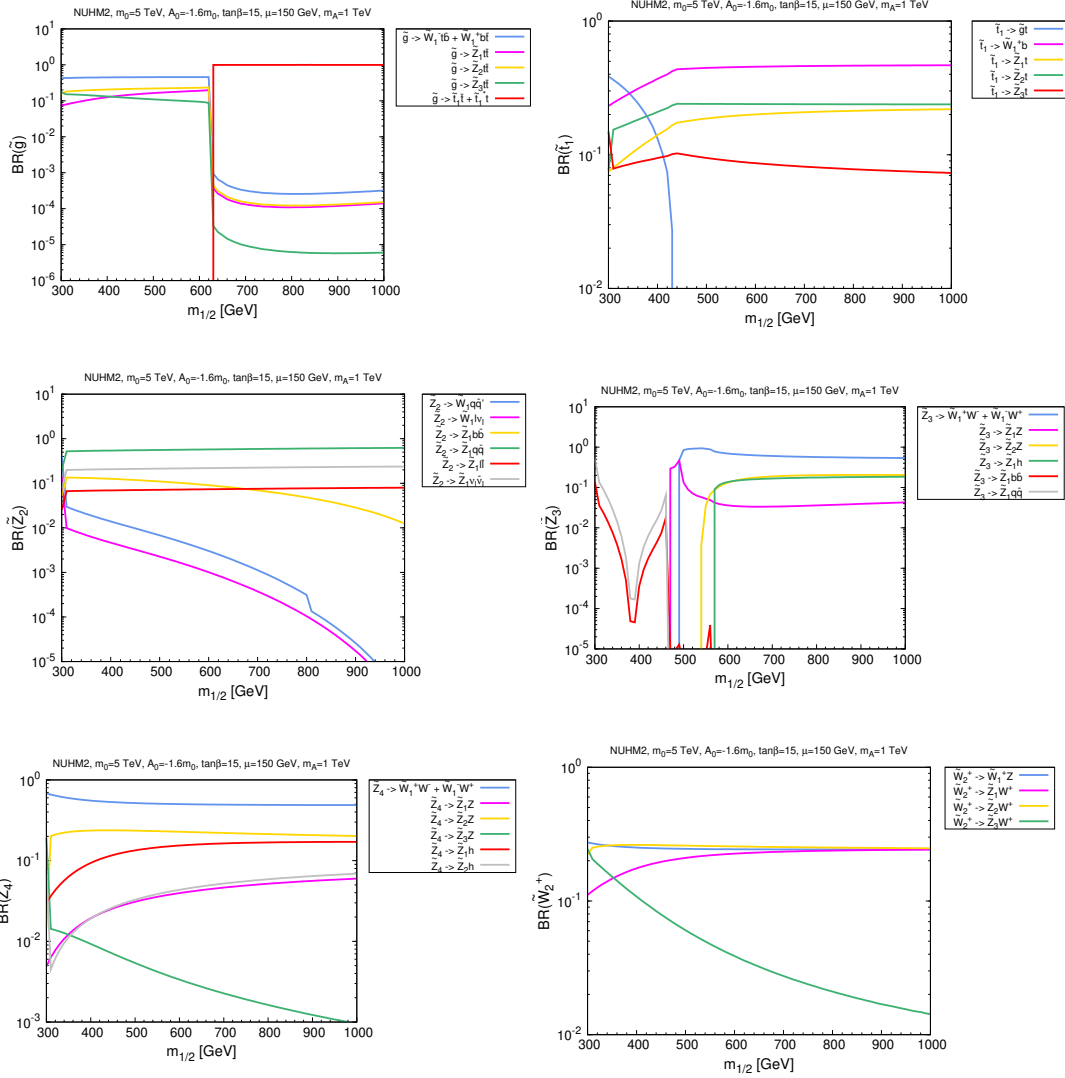


**Figure 6:** Plot of various particle branching fractions versus  $m_{1/2}$  along the RNS model line.

mode is open and is dominant. However, as  $m_{1/2}$  increases, this mode quickly closes and instead  $\tilde{t}_1$  decays into  $b\tilde{W}_1$  or  $t\tilde{Z}_{1,2,3}$ .

In frame c), we show the  $\tilde{Z}_2$  decay modes. Since the  $m_{\tilde{Z}_2} - m_{\tilde{Z}_1}$  mass gap ranges from  $\sim 55$  GeV (already excluded for this model line by LHC8 gluino searches) to  $\sim 10$  GeV along the model line, then  $\tilde{Z}_2$  always decays dominantly to 3-body modes  $\rightarrow \tilde{W}_1 f \bar{f}'$  or  $\rightarrow \tilde{Z}_1 f \bar{f}$ , where  $f$  stands for kinematically accessible SM fermions. As mentioned earlier, since the  $\tilde{Z}_2 - \tilde{Z}_1$  mass gap is small and the released decay energy is shared between three particles, then the decay products from  $\tilde{Z}_2$  decay are usually very soft – in the few GeV range. The light chargino (branching fractions not shown) decays into  $\tilde{Z}_1 f \bar{f}'$  mainly via  $W^*$ , where the  $f$  and  $\bar{f}'$  are again typically rather soft.

In frame d) we show the bino-like  $\tilde{Z}_3$  decays. Here  $\tilde{Z}_3 \rightarrow \tilde{W}_1 f \bar{f}'$  or  $\tilde{Z}_{1,2} f \bar{f}$  for  $m_{1/2} \lesssim$

Particle	dom. mode	BF
$\tilde{g}$	$\tilde{t}_1 t$	$\sim 100\%$
$\tilde{t}_1$	$b\tilde{W}_1$	$\sim 50\%$
$\tilde{Z}_2$	$\tilde{Z}_1 f \bar{f}$	$\sim 100\%$
$\tilde{Z}_3$	$\tilde{W}_1^\pm W^\mp$	$\sim 50\%$
$\tilde{Z}_4$	$\tilde{W}_1^\pm W^\mp$	$\sim 50\%$
$\tilde{W}_1$	$\tilde{Z}_1 f \bar{f}'$	$\sim 100\%$
$\tilde{W}_2$	$\tilde{Z}_i W$	$\sim 50\%$

**Table 1:** Dominant branching fractions of various sparticles along the RNS model line for  $m_{1/2} = 1$  TeV.

500 GeV. For heavier  $m_{\tilde{Z}_3} \gtrsim 220$  GeV (this value, of course, depends on our choice of  $\mu$ ), the 2-body decays  $\tilde{Z}_3 \rightarrow \tilde{W}_1^\pm W^\mp$  and  $\tilde{Z}_{1,2} Z$  and  $\tilde{Z}_1 h$  turn on, leading to production of vector bosons and Higgs bosons in the SUSY events.

In frames *e*) and *f*), we show the neutral  $\tilde{Z}_4$  and charged  $\tilde{W}_2^\pm$  wino branching fractions. We see that  $\tilde{Z}_4 \rightarrow \tilde{W}_1^\pm W^\mp$  mode dominates over the entire range of  $m_{1/2}$ . The subdominant decay modes  $\tilde{Z}_4 \rightarrow \tilde{Z}_{1,2} Z$  and  $\tilde{Z}_{1,2} h$  can also be important and occur at significant rates. The sizeable branching ratio for the decay  $\tilde{Z}_4 \rightarrow Z \tilde{Z}_1$  may be surprising at first glance since  $\tilde{Z}_4$  is dominantly a wino while  $\tilde{Z}_1$  is mostly a higgsino, so that the  $Z \tilde{Z}_4 \tilde{Z}_1$  coupling should be suppressed by the small higgsino content  $\sim M_Z/M_2$  (assuming  $M_2 \gg |\mu|$ ) of  $\tilde{Z}_4$ . For heavy  $\tilde{Z}_4$ , this suppression is compensated for by the fact that the amplitude for decay to the *longitudinally polarized*  $Z$  boson is enhanced by  $\sim |\mu|/M_Z$ . As a result, for  $M_2 \gg M_Z, |\mu|$ , the branching fractions for decays to  $Z$  and to  $h$  become comparable. This is discussed in detail in Ref. [32]. In the case of  $\tilde{W}_2$  decay shown in frame *f*), we see that  $\tilde{W}_2 \rightarrow \tilde{W}_1 Z$  or  $\tilde{Z}_{1,2} W$  or  $\tilde{W}_1 h$  over the entire range of  $m_{1/2}$ , leading again to production of gauge and Higgs bosons in wino pair production events. The dominant sparticle branching fractions for  $m_{1/2} = 1$  TeV along the RNS model line are shown in Table 1.

#### 4. Gluino cascade decay signatures

We first examine the  $pp \rightarrow \tilde{g} \tilde{g} X$  reaction followed by gluino cascade decays[33] which can be searched for in multi-lepton plus multi-jet  $+E_T^{\text{miss}}$  events. We neglect squark pair production and gluino-squark associated production which occur at very low rates because squarks are heavy.

We use Isajet 7.83 [20] for the generation of signal events at LHC14. For event generation, we use a toy detector simulation with calorimeter cell size  $\Delta\eta \times \Delta\phi = 0.05 \times 0.05$  and  $-5 < \eta < 5$ . The HCAL (hadronic calorimetry) energy resolution is taken to be  $80\%/\sqrt{E} + 3\%$  for  $|\eta| < 2.6$  and FCAL (forward calorimetry) is  $100\%/\sqrt{E} + 5\%$  for  $|\eta| > 2.6$ , where the two terms are combined in quadrature. The ECAL (electromagnetic calorimetry) energy resolution is assumed to be  $3\%/\sqrt{E} + 0.5\%$ . We use the cone-type Isajet jet-finding

algorithm [20] to group the hadronic final states into jets. Jets and isolated leptons are defined as follows:

- Jets are hadronic clusters with  $|\eta| < 3.0$ ,  $R \equiv \sqrt{\Delta\eta^2 + \Delta\phi^2} \leq 0.4$  and  $E_T(jet) > 50$  GeV.
- Electrons and muons are considered isolated if they have  $|\eta| < 2.5$ ,  $p_T(l) > 10$  GeV with visible activity within a cone of  $\Delta R < 0.2$  about the lepton direction,  $\Sigma E_T^{cells} < 5$  GeV.
- We identify hadronic clusters as  $b$ -jets if they contain a B hadron with  $E_T(B) > 15$  GeV,  $\eta(B) < 3$  and  $\Delta R(B, jet) < 0.5$ . We assume a tagging efficiency of 60% and light quark and gluon jets can be mis-tagged as a  $b$ -jet with a probability 1/150 for  $E_T \leq 100$  GeV, 1/50 for  $E_T \geq 250$  GeV, with a linear interpolation for intermediate  $E_T$  values.

Gluino pair production cascade decay signatures have been previously calculated and compared against backgrounds in Ref. [18]. In that paper, it was advocated that in models where gluino pair production signatures are dominant above background (such as the focus point region of mSUGRA), if one can suppress the background entirely, then the remaining total cross section may be used to extract the gluino mass to 10-15% precision. We adopt the cuts from that paper and compare RNS signal rates along the model line against previously calculated backgrounds using the exact same set of cuts.

In Ref. [18], the following pre-cuts set  $C1$  are first invoked[34]:

**C1 Cuts:**

$$\begin{aligned}
E_T^{\text{miss}} &> \max(100 \text{ GeV}, 0.2M_{eff}), \\
n(jets) &\geq 4, \\
E_T(j_1, j_2, j_3, j_4) &> 100, 50, 50, 50 \text{ GeV}, \\
S_T &> 0.2, \\
p_T(\ell) &> 20 \text{ GeV}.
\end{aligned} \tag{4.1}$$

Here,  $M_{eff}$  is defined as in Hinchliffe *et al.*[34] as  $M_{eff} = E_T^{\text{miss}} + E_T(j_1) + E_T(j_2) + E_T(j_3) + E_T(j_4)$ , where  $j_1 - j_4$  refer to the four highest  $E_T$  jets ordered from highest to lowest  $E_T$ ,  $E_T^{\text{miss}}$  is missing transverse energy and  $S_T$  is transverse sphericity. The SM cross sections in fb after C1 cuts are listed in Table III of Ref. [18]. It is found that the signal with these cuts is swamped by various SM backgrounds (BG), especially those from QCD multi-jet production and  $t\bar{t}$  production. After inspection of a variety of distributions including jet multiplicity  $n(jets)$ ,  $b$ -jet multiplicity  $n(b-jets)$  and augmented effective mass  $A_T$  (here,  $A_T = E_T^{\text{miss}} + \sum_{leptons} E_T + \sum_{jets} E_T$ ), for  $0\ell$  and  $1\ell$  events, we amend  $C1$  cuts to

**C2 Cuts:**

$$\begin{aligned}
&\text{apply cuts set } C1 \\
n(jets) &\geq 7 \\
n(b-jets) &\geq 2 \\
A_T &\geq 1400 \text{ GeV}.
\end{aligned}$$

For multi-lepton events (opposite sign dileptons  $OS$ , same sign dileptons  $SS$  and trileptons  $3\ell$ ), we use somewhat softer cuts:

**C3 Cuts:**

$$\begin{aligned} & \text{apply cuts set } C1 \\ & n(\text{isol. leptons}) \geq 2 \\ & n(\text{jets}) \geq 4 \\ & n(b - \text{jets}) \geq 2 \\ & A_T \geq 1200 \text{ GeV}. \end{aligned}$$

After  $C2$  cuts, it is found that 1 fb of BG remains in the  $1\ell + \text{jets}$  channel and 0.5 fb of BG remains in the  $0\ell + \text{jets}$  channel. No BG was found in the  $OS + \text{jets}$ ,  $SS + \text{jets}$  or  $3\ell + \text{jets}$  channels after cuts  $C3$ . The signal rates along the RNS model line are shown in Fig. 7. From the plot, we can read off the  $5\sigma$  discovery level for various integrated luminosity choices for different signal channels. For the  $0\ell + \text{jets}$  channel with  $300 \text{ fb}^{-1}$ , we expect a reach to  $m_{1/2} \sim 650 \text{ GeV}$  corresponding to  $m_{\tilde{g}} \sim 1.7 \text{ TeV}$ . We do not project the reach in the lower background multilepton channels as these would depend on the residual background that remains.

**NUHM2:  $m_0=5 \text{ TeV}$ ,  $A_0=-1.6m_0$ ,  $\tan\beta=15$ ,  $\mu=150 \text{ GeV}$ ,  $m_A=1 \text{ TeV}$**

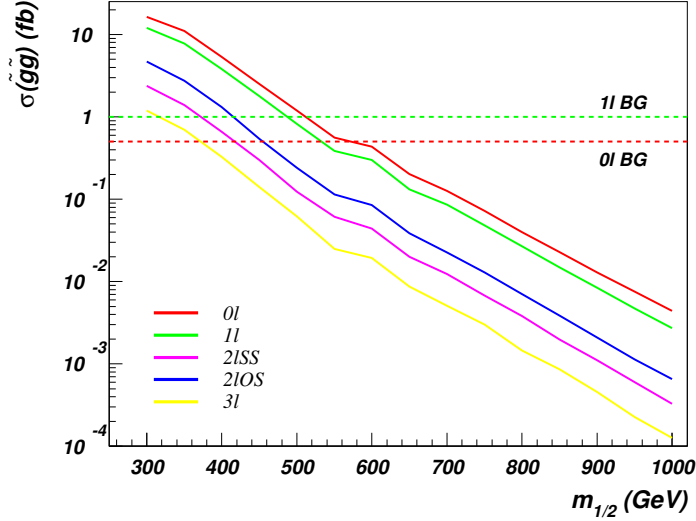


**Figure 7:** Plot of gluino cross section in  $fb$  after cuts  $C2$  for  $1\ell + \text{jets}$  and  $0\ell + \text{jets}$  channel and cuts  $C3$  for  $OS$ ,  $SS$  and  $3\ell + \text{jets}$  channels from gluino cascade decays along the RNS model line at LHC14. The horizontal lines denote the corresponding backgrounds estimated in Ref. [18].

#### 4.1 OS/SF dilepton mass distribution from cascade decays

Within the  $OS$  dileptons plus jets channel, we expect a large fraction of signal events to contain an  $OS$  dilepton pair arising from  $\tilde{Z}_2 \rightarrow \ell^+ \ell^- \tilde{Z}_1$  decay. For these events, the

$m(\ell^+\ell^-)$  distributions will be bounded by the kinematic mass difference  $m_{\tilde{Z}_2} - m_{\tilde{Z}_1} < M_Z$ . In Fig. 8, we show the invariant mass of opposite-sign/same-flavor dilepton pairs from the  $OS + jets$  events which survive cuts  $C3$ . In the figure we take  $m_{1/2} = 450$  GeV for which  $m_{\tilde{g}} = 1250$  GeV and  $m_{\tilde{Z}_2} - m_{\tilde{Z}_1} = 32$  GeV. A mass edge at 32 GeV is clearly visible from the plot, as is the  $Z$  peak. A detection of an excess of events with a cut-off on the dilepton mass could readily be attributed to neutralinos of SUSY.

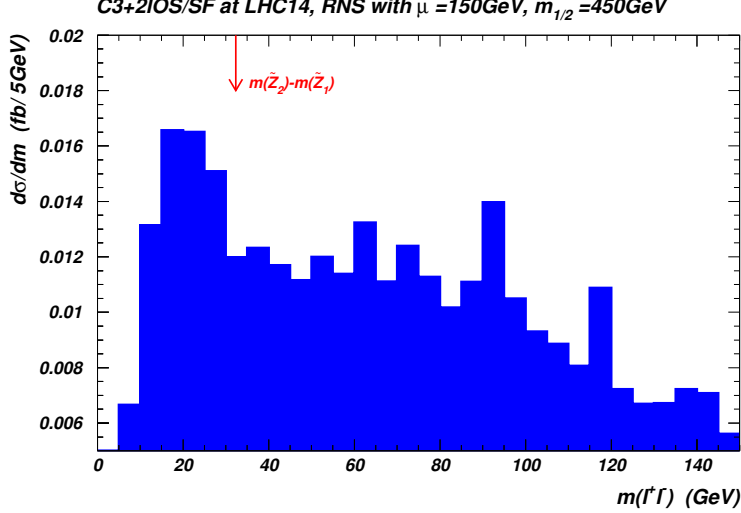


**Figure 8:** Distribution of the invariant mass of opposite-sign/same-flavor dileptons after cuts  $C3$  at LHC14 from the RNS benchmark model line with  $m_{1/2} = 450$  GeV.

## 5. Same-sign diboson signature

In this Section, we revisit and present further details on the same-sign diboson (SSdB) signature which was first introduced in Ref. [17]. The idea here is that in models where  $|\mu|$  is smaller than the magnitude of gaugino mass parameters – as exemplified by the RNS model line – wino pair production provides a novel signature with a final state characterized by two same sign  $W$  bosons and  $E_T^{\text{miss}}$  but accompanied by just modest jet activity. The most promising reaction appears to be  $pp \rightarrow \tilde{W}_2^\pm \tilde{Z}_4$ , where  $\tilde{W}_2^\pm \rightarrow W^\pm \tilde{Z}_{1,2}$  and  $\tilde{Z}_4 \rightarrow W^\pm \tilde{W}_1^\mp$  although  $\tilde{W}_2^+ \tilde{W}_2^-$  pair production also provides a non-negligible signal contribution. We see from Fig. 6 that the winos have substantial branching fractions for decays to  $W$  bosons. For these decays, half the time the final states consist of  $W^\pm W^\pm + E_T^{\text{miss}}$ . We focus our attention on the SS dilepton signal from the leptonic decays of both  $W$ s. The jet activity in these events is relatively limited since the daughter higgsinos  $\tilde{W}_1$  and  $\tilde{Z}_{1,2}$  usually yield only soft decay products. This serves to distinguish the wino-pair induced SSdB signature from the SS dilepton signal from gluino pair production – the latter is expected to be accompanied by several hard jets.

The SM physics backgrounds to the SSdB signal come from  $uu \rightarrow W^+ W^+ dd$  or  $dd \rightarrow W^- W^- uu$  production with a cross section  $\sim 350$  fb. These events will be characterized



by high rapidity (forward) jets and rather low  $E_T^{\text{miss}}$ .  $W^\pm W^\pm$  pairs may also occur via two overlapping events: such events will mainly have low  $p_T$   $W$ s and possibly distinct production vertices. Double parton scattering will also lead to SSdB events at a rate somewhat lower than the  $qq \rightarrow W^\pm W^\pm q'q'$  process[35]. Additional physics backgrounds come from  $t\bar{t}$  production where a lepton from a daughter  $b$  is accidentally not isolated, from  $t\bar{t}W$  production and from  $4t$  production. SM processes such as  $WZ \rightarrow 3\ell$  and  $t\bar{t}Z \rightarrow 3\ell$  production, where one lepton is missed, constitute *reducible* backgrounds to the signal.

Here, we assume that the  $2 \rightarrow 4$  processes as well as the double parton scattering processes, which have different characteristics from the signal, can be readily eliminated by suitable cuts and do not simulate these. For the simulation of the remaining background events we use AlpGen [36] and MadGraph 5 [37] to generate the hard scattering events. Those events are then passed to Pythia 6.4 [38] via the LHE interface [39] for showering and hadronization. For the  $2 \rightarrow 4$  “ $WZ$ ” process, we compute the full matrix element for  $pp \rightarrow l^+l^-l'\nu'$  that includes contributions from on- and off-shell  $Z$  and  $\gamma$  as well as from interference diagrams. We normalize signal and background to NLO cross sections obtained with Prospino [25] and MCFM [40], respectively. To reconstruct jets and isolated leptons we followed the procedure described in Sec. 4.

In Ref. [17], the following cuts were imposed:

- *exactly* 2 isolated same-sign leptons with  $p_T(\ell_1) > 20$  GeV and  $p_T(\ell_2) > 10$  GeV,
- $n(b - \text{jets}) = 0$  (to aid in vetoing  $t\bar{t}$  background).

After these cuts, the event rate is dominated by  $WZ$  and  $t\bar{t}$  backgrounds.

To distinguish signal from background, we next construct the transverse mass of each lepton with  $E_T^{\text{miss}}$ :

$$m_T^{\min} \equiv \min [m_T(\ell_1, E_T^{\text{miss}}), m_T(\ell_2, E_T^{\text{miss}})] . \quad (5.1)$$

The signal gives rise to a continuum distribution, whilst the dominant backgrounds have a kinematic cut-off around  $m_T^{\min} \simeq M_W$  (as long as the  $E_T^{\text{miss}}$  dominantly arises from the leptonic decay of a single  $W$ ). The situation is shown in Fig. 9, where we show in *a*) the  $m_T^{\min}$  distribution, while in *b*) we show the  $E_T^{\text{miss}}$  distribution. The bulk of  $t\bar{t}$  and  $WZ$  backgrounds can be eliminated by requiring

- $m_T^{\min} > 125$  GeV and
- $E_T^{\text{miss}} > 200$  GeV.

After these cuts, we are unable to generate any background events from  $t\bar{t}$  and  $WZ$  production, where the 1-event level in our simulation was 0.05 fb and 0.023 fb, respectively. The dominant SM background for large  $m_T^{\min}$  then comes from  $Wt\bar{t}$  production for which we find (including a QCD  $k$ -factor  $k = 1.18$  obtained from Ref. [41]) a cross section of 0.019 (0.006) fb after the cuts  $m_T^{\min} > 125$  (175) GeV and  $E_T^{\text{miss}} > 200$  GeV; the harder cuts serve to optimize the signal reach for high  $m_{1/2}$  values.<sup>4</sup>

---

<sup>4</sup>We have ignored detector-dependent backgrounds from jet-lepton misidentification in our analysis, but are optimistic that these can be controlled by the  $m_T^{\min}$  and  $E_T^{\text{miss}}$  cuts. Estimates of the background from charge mis-identification, which could be important, especially for electrons, are also beyond the scope of this analysis.

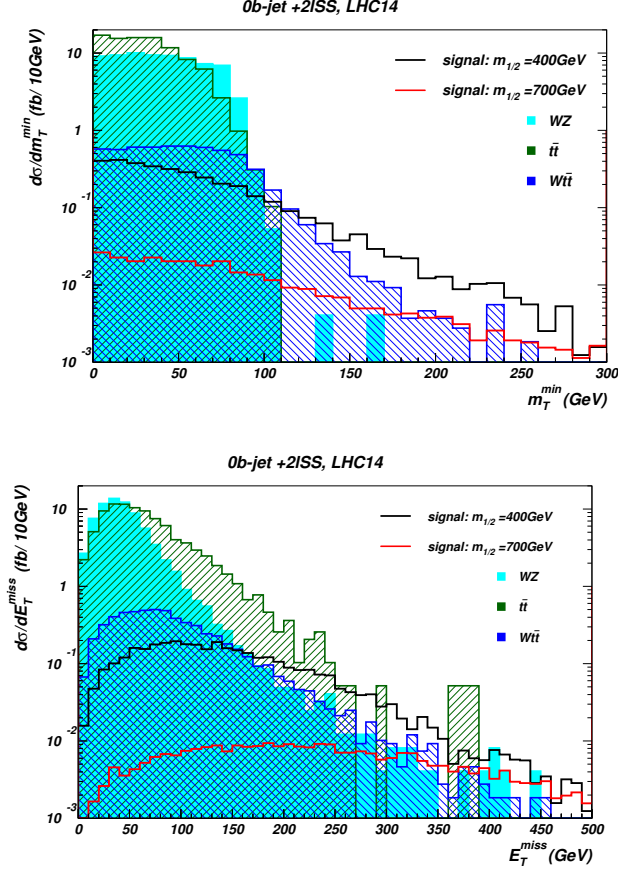


**Figure 9:** Transverse mass and missing energy distributions for SSdB events after cuts at LHC14. The open black and red histograms represent the signal from winos – via  $\widetilde{W}_2\widetilde{Z}_4$  and  $\widetilde{W}_2^+\widetilde{W}_2^-$  pair production – for the RNS model-line points with  $m_{1/2} = 400$  GeV and 700 GeV, respectively.

The calculated signal rates after cuts along the RNS model line from just  $\widetilde{W}_2^\pm\widetilde{Z}_4$  and  $\widetilde{W}_2^\pm\widetilde{W}_2^\mp$  production are shown vs.  $m_{1/2}$  in Fig. 10 where the upper (blue) curves require  $m_T^{\min} > 125$  GeV and the lower (orange) curve requires  $m_T^{\min} > 175$  GeV. The  $\widetilde{W}_2\widetilde{Z}_4$  and  $\widetilde{W}_2\widetilde{W}_2$  cross sections are normalized to those from Prospino[25]. For observability with an assumed value of integrated luminosity, we require: 1) significance  $> 5\sigma$ , 2) Signal/BG  $> 0.2$  and 3) at least 5 signal events. The LHC signal (blue dashed curve) and reach lines for integrated luminosity values 25 and 100  $\text{fb}^{-1}$  with a soft  $E_T^{\text{miss}} > 75$  GeV cut are shown first. The 25  $\text{fb}^{-1}$  reach is to  $m_{1/2} \simeq 450$  GeV corresponding to gluinos of  $\sim 1300$  GeV. As greater integrated luminosity is accumulated, harder cuts can be applied. The solid blue line shows signal for  $E_T^{\text{miss}} > 200$  GeV and reach for 100, 300 and 1000  $\text{fb}^{-1}$ . With harder cuts, the 100  $\text{fb}^{-1}$  reach extends to  $m_{1/2} \simeq 680$  GeV corresponding to  $m_{\tilde{g}} \sim 1.75$  TeV in a model with gaugino mass unification. The direct search for  $\tilde{g}\tilde{g}$  gives a projected reach of  $m_{\tilde{g}} \sim 1.6$  TeV as we have seen in Sec. 4; see also Ref. [42]. Thus, with  $\mathcal{O}(100)$   $\text{fb}^{-1}$  of integrated luminosity, the SS diboson signal offers a comparable reach to that for gluino cascade decays. For 300 (1000)  $\text{fb}^{-1}$  of integrated luminosity, the reach is improved with

a harder  $m_T^{\min} > 175$  GeV cut. In this case, we find the LHC14 reach for SS dibosons extends to  $m_{1/2} \sim 840$  (1000) GeV, corresponding to  $m_{\tilde{g}}$  of 2.1 and 2.4 TeV. For the RNS model-line where gaugino mass unification is assumed, these reach numbers extend well beyond the LHC14 reach for direct gluino pair production[43]. Regardless of this, we emphasize that the SSdB signal is a new independent signal, and detection of signals in multiple channels will be essential to unravel the underlying origin of any new physics that is found.

**NUHM2:  $m_0=5$  TeV,  $A_0=-1.6m_0$ ,  $\tan\beta=15$ ,  $\mu=150$  GeV,  $m_A=1$  TeV**

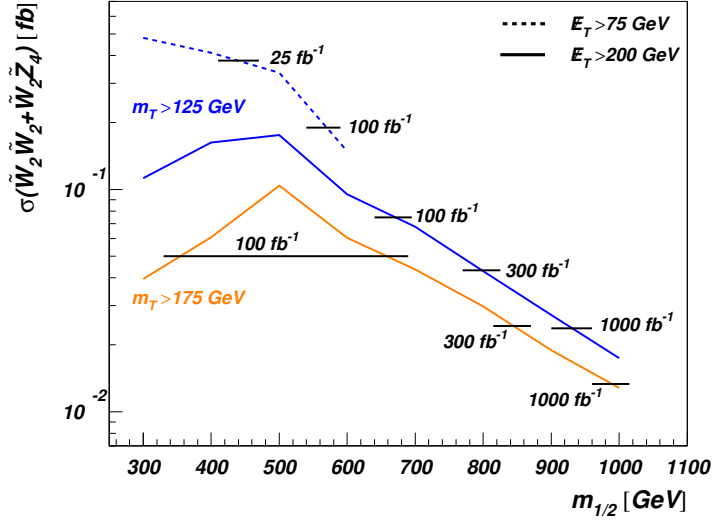


**Figure 10:** Same-sign dilepton cross sections (in  $fb$ ) at LHC14 after cuts vs.  $m_{1/2}$  along the RNS model line from  $\tilde{W}_2^\pm \tilde{Z}_4$  and  $\tilde{W}_2^\pm \tilde{W}_2^\mp$  production and calculated reach for 100, 300 and 1000  $fb^{-1}$ . The upper solid and dashed (blue) curves requires  $m_T^{\min} > 125$  GeV while the lower solid (orange) curve requires  $m_T^{\min} > 175$  GeV. The signal is observable above the horizontal lines.

We stress again that the low jet activity associated with the SSdB signal from SUSY models with light higgsinos makes it quite distinct from the usual SS dilepton signal arising from gluino pair production, which is usually accompanied by numerous hard jets and high  $E_T^{\text{miss}}$ . Recent CMS searches for SS dileptons from SUSY[44] required the presence of multiple jets (some  $b$ -tagged jets) or large  $H_T$  in the events; these cuts greatly reduce or even eliminate our SSdB signal. Likewise, the cuts  $n_j \geq 3$  high  $p_T$  jets (possibly  $b$ -tagged) along with  $E_T^{\text{miss}} > 150$  GeV and large  $m_{\text{eff}}$  required by a recent ATLAS search for SS dileptons from gluinos[45] would have eliminated much of the SSdB signal from SUSY with light higgsinos.

Hard trilepton production from winos (discussed in the next section) can lead to clean, same-sign dilepton events if a lepton is not isolated or fails to be identified. The CMS collaboration used this channel to extend the search for electroweak-inos to portions of parameter space not accessible via the trilepton search, requiring  $120 \text{ GeV} < E_T^{\text{miss}} <$

200 GeV [46]. They do not, however, impose the  $m_T^{\min}$  cut that we found crucial for our SSdB analysis. The CMS search is thus not optimized for the clean SS dilepton signal in the RNS scenario. In any case, with just  $\sim 20 \text{ fb}^{-1}$  at LHC8, this channel should have a lower reach than that via multi-jet plus multi-lepton events from gluino pair production.

## 6. Hard trileptons from wino pair production

In this Section, we examine prospects for detection of reactions such as

$$pp \rightarrow \widetilde{W}_2 \widetilde{Z}_4 \rightarrow (\widetilde{W}_1 Z) + (\widetilde{W}_1 W) \rightarrow WZ + E_T^{\text{miss}} \rightarrow \ell^+ \ell^- \ell' + E_T^{\text{miss}}. \quad (6.1)$$

The trilepton channel where the neutralino decays via the three-body decay  $\widetilde{Z}_2 \rightarrow \ell^+ \ell^- \widetilde{Z}_1$  because the two-body decay  $\widetilde{Z}_2 \rightarrow Z \widetilde{Z}_1$  is kinematically forbidden (so that SM trileptons from  $WZ$  production can be eliminated via a mass cut on the opposite-sign, same flavour dilepton pair) has long been regarded as a golden channel in the search for gauginos from supersymmetry [47]. More recently, it has been pointed out [48] that at least within mSUGRA the trilepton search for gauginos is viable even when the neutralinos decay to on-shell  $Z$  bosons. Indeed, the CMS and ATLAS experiments have searched in this channel and found that there is no excess above SM expectations [49]. For a recent assessment of multilepton signals, see Ref. [32]. Here, we analyse prospects for this signal for the RNS model line for the most part following the cuts of Ref. [48] which required:

### Pre-Selection Cuts:

- $n(b - jets) = 0$  (to aid in vetoing  $t\bar{t}$  background),
- 3 isolated leptons with  $p_T(\ell) > 20 \text{ GeV}$  and
- $|m(\ell^+ \ell^-) - M_Z| < 10 \text{ GeV}$  (leptonic  $Z$ ),

where two of the leptons in the event must form an OS/SF pair. If more than one OS/SF pairing is possible, the pair which minimizes  $|m(\ell^+ \ell^-) - M_Z|$  is chosen. The remaining lepton is labeled  $\ell'$ . In the case of the RNS model line, the  $WZ + E_T^{\text{miss}}$  signal also receives a smaller, though non-negligible contribution, from  $\widetilde{W}_2^+ \widetilde{W}_2^-$  where one of the winos decays via  $\widetilde{W}_2 \rightarrow W \widetilde{Z}_{1,2}$  and the other via  $\widetilde{W}_2 \rightarrow Z \widetilde{W}_1$  mode. At this point, a large background from the  $2 \rightarrow 4$  process  $pp \rightarrow (\ell^+ \ell^-) + (\ell^{\pm'} \nu_{\ell'})$  which occurs via various on- and off-shell processes – including  $W^* Z^*$  and  $W^* \gamma^*$  production – tends to dominate the signal. Here, we re-evaluate the  $2 \rightarrow 4$  process using MadGraph with no restriction on the invariant mass around the  $Z$  and  $W$  resonances.<sup>5</sup> For  $t\bar{t}$ ,  $Z(l\bar{l}) + jets$ ,  $W(l\nu) + jets$ ,  $Z(l\bar{l}) + t\bar{t}$  and  $W(l\nu) + t\bar{t}$  (all summed over 3 lepton flavors) we allow for at least two additional partons in the final state and use the MLM matching scheme [50] to avoid double counting. We have also included  $ZZ$ ,  $W(l\nu) + tb$  and  $Z(l\bar{l}) + b\bar{b}$  backgrounds. The signal and background distributions in  $m_T(\ell', E_T^{\text{miss}})$  and  $E_T^{\text{miss}}$  are shown in Fig. 11.

To enhance the signal relative to background, we then require,

---

<sup>5</sup>The  $WZ$  background after all cuts in Table 1 of Ref. [48] has been underestimated by a factor of about 2.5 because the virtual  $W$ -mass did not extend to large enough values, leading to an under-estimate of the tail of the  $m_T$  distribution.

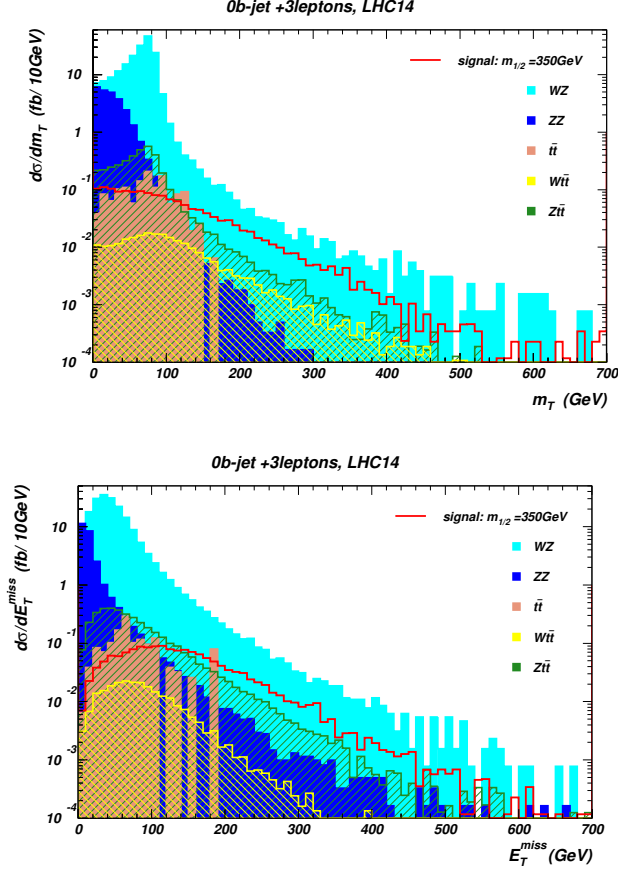


**Figure 11:** Transverse mass and missing energy distributions for hard trilepton events after the preliminary cuts at LHC14. The open red histograms represent the signal from winos,  $\tilde{W}_2$  and  $\tilde{Z}_4$ , for the RNS point with  $m_{1/2} = 350$  GeV.

- $m_T(\ell', E_T^{\text{miss}}) > 125$  GeV,
- $E_T^{\text{miss}} > 150$  GeV.

The  $m_T$  cut is as in Ref. [48], but for the larger integrated luminosity and concomitantly higher wino masses that we are considering here, we found that stiffening the  $E_T^{\text{miss}}$  cut yields a better signal-to-background ratio. The background from various SM sources along with RNS signal for  $m_{1/2} = 350$  GeV is shown after cuts in Table 2 for LHC14.

In Fig. 12, we show the  $3\ell + E_T^{\text{miss}}$  signal cross section after all cuts versus  $m_{1/2}$  along the RNS model line. The turn-over at the left end of the curve is because of the efficiency loss resulting from the stiff  $E_T^{\text{miss}}$  cut which is optimized to yield the best reach for high wino masses. For  $100 \text{ fb}^{-1}$  of integrated luminosity, there is no reach, while the reach in  $m_{1/2}$  is shown for 300 and 1000  $\text{fb}^{-1}$ . The 300  $\text{fb}^{-1}$  reach extends to  $m_{1/2} = 500$  GeV while the 1000  $\text{fb}^{-1}$  reach extends to  $m_{1/2} = 630$  GeV. These values correspond to gluino masses of  $m_{\tilde{g}} = 1.3$  TeV and 1.65 TeV, respectively. These reaches are smaller than those obtained

	$t\bar{t}$	$WZ$	$ZZ$	$Z + t\bar{t}$	$W + t\bar{t}$	Total BG	Signal
Events Generated	12M	1.5M	1M	1.2M	10M		200K
$n(b) = 0, n(l) = 3$	6.96	211.94	26.07	4.26	1.84	247.29	2.88
OS/SF pair	5.25	211.51	26.02	4.21	1.37	251.97	2.57
$m(\ell^+\ell^-)$ cut	0.95	186.90	25.55	3.99	0.24	221.20	1.52
$m_T > 125$ GeV	0.03	1.64	0.05	0.20	0.07	1.99	0.43
$E_T^{\text{miss}} > 150$ GeV	0.006	0.24	$< 0.00085$	0.0058	0.016	0.32	0.22

**Table 2:** Number of events generated and cross section after cuts for the dominant backgrounds in the hard trilepton channel and for the RNS signal with  $m_{1/2} = 350$  GeV. All cross sections are in  $fb$ . The total BG values include all processes listed in the text, including the subdominant ones not shown in the Table.

from the  $\tilde{g}\tilde{g}$  and SSdB signals. They would, nevertheless, offer corroborative evidence for any SUSY discovery at the lower range of allowed  $m_{1/2}$  values.

**NUHM2:  $m_0=5$  TeV,  $A_0=-1.6m_0$ ,  $\tan\beta=15$ ,  $\mu=150$  GeV,  $m_A=1$  TeV**

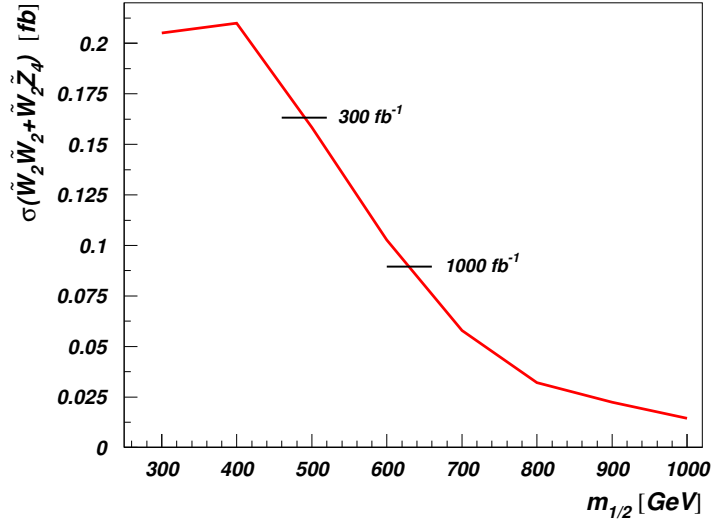


**Figure 12:** Tri-lepton cross sections (in  $fb$ ) at LHC14 after cuts vs.  $m_{1/2}$  along the RNS model line from wino pair production processes  $pp \rightarrow \tilde{W}_2 \tilde{Z}_4 / \tilde{W}_2 \tilde{W}_2 \rightarrow WZ + E_T^{\text{miss}} \rightarrow 3\ell + E_T^{\text{miss}}$  events.

## 7. Four leptons from heavy gaugino production

We saw in Fig. 6 that the wino-like  $\tilde{W}_2$  and  $\tilde{Z}_4$  have significant branching fractions to  $W$  and  $Z$  bosons resulting in the dilepton and trilepton signals already discussed. A small fraction of the time, there may be two  $Z$  bosons in these events, leading to the possibility of a four-lepton signal. Additional leptons can arise from the leptonic decays of daughter

$\widetilde{W}_1$  and  $\widetilde{Z}_2$ . Although the decay products are generally soft, the ubiquity of these light higgsino-like states within the RNS framework often results in additional detectable leptons ( $e$  and  $\mu$ ) in would-be trilepton events. This characteristic feature of low  $|\mu|$  models such as RNS is absent in models such as mSUGRA that have received the most attention in the literature, and leads to the possibility of four-lepton plus  $E_T^{\text{miss}}$  signal, even in  $R$ -parity conserving SUSY.<sup>6</sup> A study of this new signal for which we require

- 4 isolated leptons with  $p_T(\ell) > 10$  GeV within  $|\eta(\ell)| < 2.5$ ,
- $n_b = 0$ , to veto backgrounds from top decays,
- $E_T^{\text{miss}} > E_T^{\text{miss}}(\text{cut})$ , where  $E_T^{\text{miss}}(\text{cut})$  is chosen to select signal events above SM backgrounds,

forms the subject of this section.

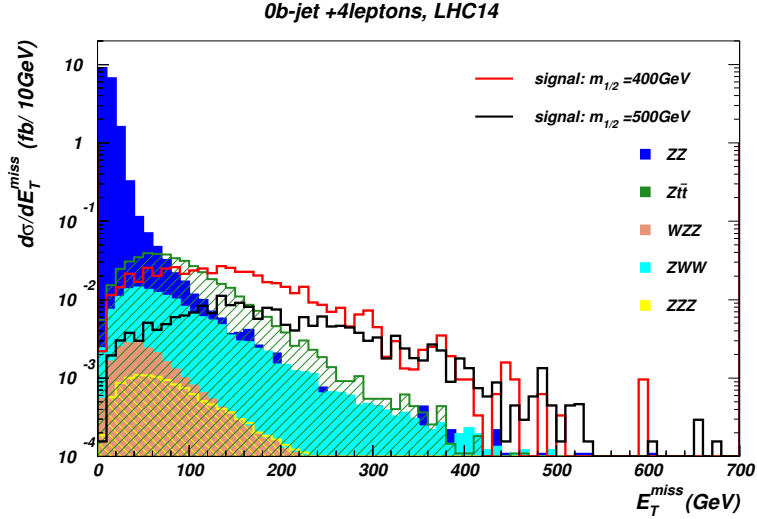


**Figure 13:** The  $E_T^{\text{miss}}$  distributions for  $4\ell$  events with  $n_b = 0$  from various SM sources and for two signal points on the RNS model-line.

Within the SM, the main sources of  $4\ell + E_T^{\text{miss}}$  events are  $ZZ$ ,  $Zt\bar{t}$ ,  $ZWW$ ,  $ZZW$ ,  $ZZZ$  and  $Zh(\rightarrow WW^*)$ , followed by leptonic decays of tops, and of the electroweak vector bosons. The bulk of the background from  $ZZ$  production is eliminated by requiring a large  $E_T^{\text{miss}}$ . Nevertheless, this background remains significant since  $E_T^{\text{miss}}$  can arise via  $Z \rightarrow \tau^+\tau^- \rightarrow \ell^+\ell'^- + E_T^{\text{miss}}$ .

We have simulated the RNS signal along with backgrounds from  $ZZ$ ,  $t\bar{t}Z$  and  $VVV$  ( $V = W, Z$ ) using AlpGen and Pythia. The cross sections for the most important of these backgrounds are listed in the second column of Table 3, together with that for the signal for three model-line points. The last two columns list these signal and background

<sup>6</sup>It is well-known that high lepton multiplicities are obtained if the LSP decays via lepton-number-violating interactions that do not conserve  $R$ -parity.

cuts	$n(b) = 0, n(l) = 4$	$E_T^{\text{miss}} > 100 \text{ GeV}$	$E_T^{\text{miss}} > 200 \text{ GeV}$
$ZZ$	18.02	0.0611	0.0094
$Zt\bar{t}$	0.450	0.158	0.0232
$ZWW$	0.155	0.0516	0.0134
Total BG	18.66	0.280	0.0483
$m_{1/2} = 400 \text{ GeV}$	0.527	0.343 ( <b>11.2</b> )	0.122 ( <b>3.8</b> )
$m_{1/2} = 500 \text{ GeV}$	0.195	0.157 ( <b>5.1</b> )	0.0769 ( <b>6.1</b> )
$m_{1/2} = 600 \text{ GeV}$	0.084	0.0728 ( <b>2.3</b> )	0.0467 ( <b>3.7</b> )

**Table 3:** Background and signal rates in  $fb$  for 4-lepton events at LHC14 after cuts. The bold-faced numbers in parenthesis in the last two columns show the statistical significance of the signal with  $300 \text{ fb}^{-1}$  of integrated luminosity at LHC14. The signal comes from wino pair production for points on the RNS model line introduced in the text.

calculations for  $E_T^{\text{miss}}(\text{cut}) = 100$  and  $200 \text{ GeV}$ , the choice being motivated by the  $E_T^{\text{miss}}$  distributions shown in Fig. 13. The numbers in bold-face show the statistical significance for an integrated luminosity of  $300 \text{ fb}^{-1}$ .

We estimate that  $Zh(\rightarrow W^\pm \ell \nu)$  yields a  $4\ell$  cross section  $\sim 1300 \text{ fb} \times 0.06 \times 0.22 \times 0.03$  (where the last factor is the branching fraction for  $h \rightarrow W^\pm \ell^\mp \nu$  decay)  $\simeq 0.5 \text{ fb}$ , before any lepton acceptance cuts which further reduce the cross section by factor about 5-10. After the hard  $E_T^{\text{miss}}$  requirement, we expect this to make a relatively unimportant contribution to the background. Backgrounds from  $ttWW$  and  $4V$  processes should also be small.

Several comments are worth noting.

- There is no benefit, and in fact a loss of significance, by requiring pairs of leptons to reconstruct to  $M_Z$ . This is largely because the largest  $4\ell$  backgrounds also all have a  $Z$  in them, and both signal and backgrounds drop roughly equally due to this requirement.
- The softer  $E_T^{\text{miss}} > 100 \text{ GeV}$  cut works better for  $m_{1/2} = 400 \text{ GeV}$  for which a  $6\sigma$  signal is obtained even with just  $100 \text{ fb}^{-1}$  of integrated luminosity.
- The  $5\sigma$  reach for  $300 \text{ fb}^{-1}$  ( $1000 \text{ fb}^{-1}$ ) extends to  $m_{1/2} = 500 \text{ GeV}$  (beyond  $m_{1/2} = 600 \text{ GeV}$ ) with the harder  $E_T^{\text{miss}}(\text{cut}) = 200 \text{ GeV}$ .

We conclude that the  $4\ell$  channel would serve to confirm a the SSdB signal pointing to light higgsinos out to  $m_{1/2}$  values  $\lesssim 500 - 650 \text{ GeV}$ , depending on the integrated luminosity that is ultimately available.

We remark that current ATLAS [51] and CMS [52] 4-lepton searches are optimized for the signal from the cascade decays of gluinos (and so do not veto hadronic activity) with the high lepton multiplicity originating in R-parity violating leptonic decays of  $\tilde{Z}_1$ . In contrast, our signal is hadronically quiet and would stand out over SM backgrounds with veto on b-jets as described in the text.



## 8. Soft trileptons from direct higgsino pair production

In this Section, we try to exploit the large cross sections for higgsino pair production from the RNS model at the LHC:  $pp \rightarrow \widetilde{W}_1 \widetilde{Z}_1$ ,  $\widetilde{W}_1^+ \widetilde{W}_1^-$ ,  $\widetilde{Z}_1 \widetilde{Z}_2$  and  $\widetilde{W}_1^\pm \widetilde{Z}_2$ . The purely hadronic+ $E_T^{\text{miss}}$  final states from higgsino pair production are expected to be buried beneath prodigious QCD backgrounds since the signal yields only soft, low  $p_T$  jets and soft  $E_T^{\text{miss}}$  spectra. Likewise, most single and dilepton signals are expected to be buried under  $W \rightarrow \ell \nu_\ell$  and  $WW$ ,  $t\bar{t}$  backgrounds respectively.

In previous related work, Ref. [53] did find a reach for mixed higgsino-gaugino  $\widetilde{W}_1 \widetilde{Z}_2 \rightarrow 3\ell$  (but not better than that via the gluino search) along the focus point region of mSUGRA at LHC14, where the dominant background came from  $t\bar{t}$  production, as opposed to studies for the Tevatron, where  $W^* Z^* \rightarrow (\ell \nu_\ell) + (\ell' \bar{\ell}')$  was dominant[54]. In the FP study of Ref. [53], the mixed gaugino-higgsino like  $\widetilde{W}_1$  and  $\widetilde{Z}_2$  had larger mass gaps, and hence harder decay products for the signal, as compared with the present case. Meanwhile, in Ref. [55], the light higgsino-world scenario was investigated, with a focus on the reaction  $pp \rightarrow \widetilde{Z}_1 \widetilde{Z}_2 \rightarrow \ell^+ \ell^- + E_T^{\text{miss}}$ . In that study, large backgrounds from  $WW$ ,  $\gamma^* \rightarrow \ell^+ \ell^-$  and  $\tau\bar{\tau}$  production thwarted the signal of low-mass, collimated OS/SF dileptons, even with  $p_T$  cuts extending down to 5 GeV. Here, we examine the clean trilepton signal from higgsino pair production. We generate signal events for several points along the RNS model line.

We will search for the  $pp \rightarrow \widetilde{W}_1 \widetilde{Z}_2 \rightarrow (e \nu_e \widetilde{Z}_1) + (\mu^+ \mu^- \widetilde{Z}_1)$  topology where we assume a dilepton trigger with  $p_T(e) > 10$  GeV and  $p_T(\mu) > 5$  GeV. Then we require:

- $10 \text{ GeV} < p_T(e) < 50 \text{ GeV}$ ,
- $5 \text{ GeV} < p_T(\mu_1) < 50 \text{ GeV}$ ,
- $5 \text{ GeV} < p_T(\mu_2) < 25 \text{ GeV}$ .

Scrutiny of a variety of distributions suggests the following cuts:

1.  $10 \text{ GeV} < m(\mu^+ \mu^-) < 75 \text{ GeV}$ ,
2.  $n(\text{jets}) = 0$  (jet-veto),
3. electron transverse mass  $m_T(e, E_T^{\text{miss}}) < 60 \text{ GeV}$ ,
4.  $25 \text{ GeV} < E_T^{\text{miss}} < 100 \text{ GeV}$ .

The signal and four background processes are shown in Table 4. In Fig. 14 we show distributions of electron  $p_T$  before cuts for two sample points on the RNS model line. We see that energy release is very small, less than  $\sim 25$  GeV, and quickly decreases with  $m_{1/2}$ . For  $m_{1/2} = 1$  TeV most of electrons have  $p_T$  less than 10 GeV, the trigger threshold.

After cut 4, the background exceeds signal by a factor of 10. The dimuon invariant mass distribution after cuts is shown in Fig. 15a) for  $m_{1/2} = 400$  GeV ( $\widetilde{Z}_2 - \widetilde{Z}_1$  mass gap at 38 GeV), b)  $m_{1/2} = 550$  GeV (mass gap at 25 GeV) and c)  $m_{1/2} = 700$  GeV (mass gap at 18 GeV). We see that the *shapes* of the dilepton mass distribution for the signal+background in frame a) differs from that of the background alone. A *shape analysis*

cuts	$t\bar{t}$	$W^*Z^*$	$ZZ$	$Wt\bar{t}$	signal
cut 1	12.4	7.6	0.15	0.1	0.42
cut 2	2.4	7.1	0.09	0.006	0.42
cut 3	1.3	4.4	0.08	0.003	0.42
cut 4	0.9	2.0	0.03	0.002	0.28

**Table 4:** Background and signal rates in  $fb$  for soft  $3\ell + E_T^{\text{miss}}$  events at LHC14 after cuts. The signal comes from higgsino pair production at  $m_{1/2} = 400$  GeV point on the RNS model line. The  $2 \rightarrow 4$  process labelled  $W^*Z^*$  includes  $\gamma^*$ ,  $Z^* \rightarrow \tau\bar{\tau}$ .

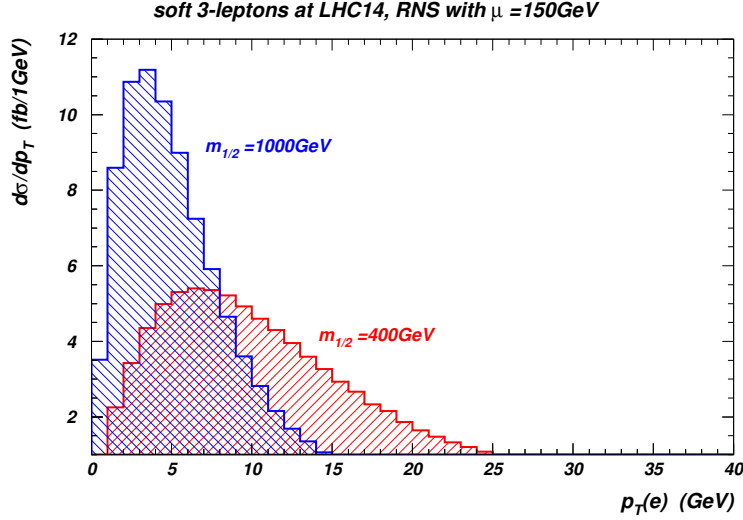


**Figure 14:**  $p_T(e)$  distribution for soft tri-leptons from higgsino pairs before cuts for two RNS points with  $m_{1/2} = 400$  GeV (red) and 1000 GeV (blue) at LHC14.

using the data at large  $m_{\ell\ell}$  to normalize the background may allow one to claim a signal, given sufficient integrated luminosity, since an excess of events should be found in bins with  $m(\mu^+\mu^-) < 38$  GeV as compared to higher mass bins where a theory-experiment match is expected. For a counting analysis alone, invoking a cut  $m(\mu^+\mu^-) < 38$  GeV, a  $5\sigma$  signal over background (without any requirement on the  $S/B$  ratio) would require about  $700 \text{ fb}^{-1}$  of integrated luminosity. In the other frames with the smaller mass gap, an excess only appears in the lowest mass bin(s) and the possibility of extracting a signal appears even more daunting.

## 9. Conclusions

Recent results from LHC7 and LHC8 have resulted in heightened concern for reconciling electroweak naturalness with lack of SUSY signals and the rather large value of  $m_h = 125$  GeV. We have argued that this reconciliation can occur within the context of radiatively-driven natural supersymmetry (or RNS) if there is a HS model that yields

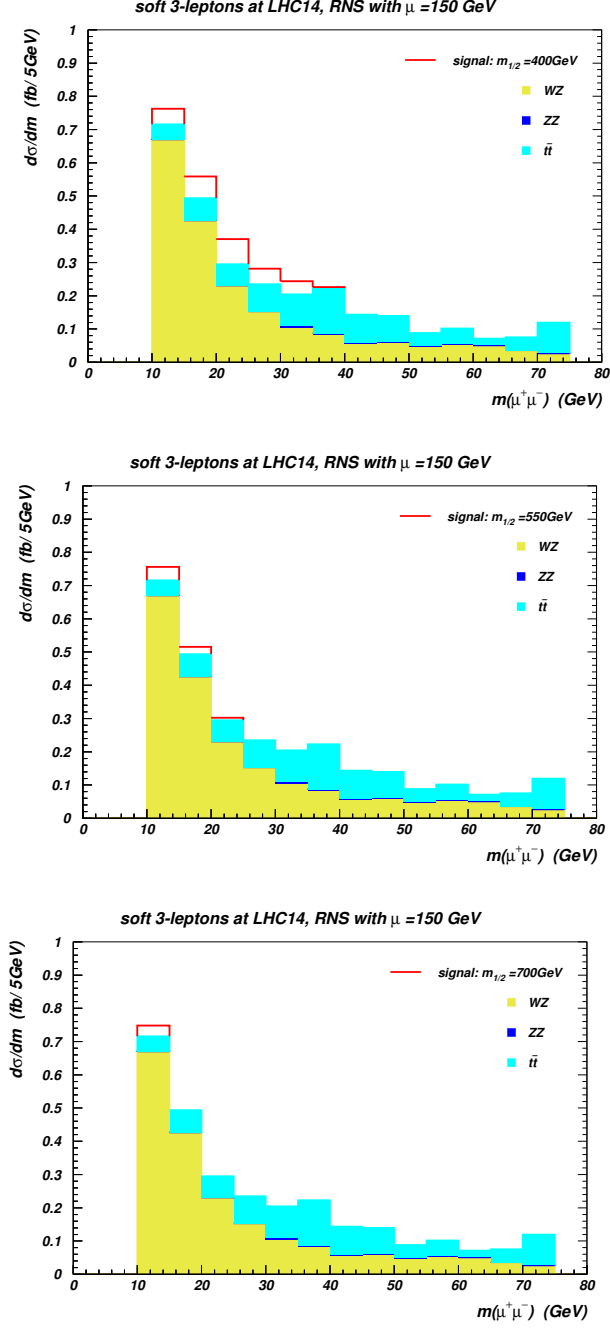


**Figure 15:** The dimuon invariant mass distributions after cuts for  $e\mu\mu$  events. Open red histograms represent signals from higgsino pair productions for three points with  $m_{1/2} = 400, 550$  and  $700$  GeV along the RNS model line.

the NUHM2 model with the required correlations between parameters as the GUT-scale effective theory, as discussed in Sec. 1. The RNS model is characterized by the presence of four light higgsinos  $\tilde{Z}_{1,2}$  and  $\tilde{W}_1^\pm$  with masses  $\sim 100 - 300$  GeV, the lower the better, fine-tuning wise. Top and bottom squarks and gluinos may lie in the 1-5 TeV range, while

Int. lum. (fb <sup>-1</sup> )	$\tilde{g}\tilde{g}$	SSdB	$WZ \rightarrow 3\ell$	$4\ell$
10	1.4	–	–	–
100	1.6	1.6	–	$\sim 1.2$
300	1.7	2.1	1.4	$\gtrsim 1.4$
1000	1.9	2.4	1.6	$\gtrsim 1.6$

**Table 5:** Reach of LHC14 for SUSY in terms of gluino mass,  $m_{\tilde{g}}$  (TeV), assuming various integrated luminosity values along the RNS model line. We present each search channel considered in this paper except soft  $3\ell$ .

first/second generation squarks and sleptons may lie in the 5-30 TeV range, thus providing at least a partial decoupling solution to the SUSY flavor and  $CP$  problems.

In this paper, we explored ways to detect RNS at the LHC with  $\sqrt{s} = 14$  TeV. To this end, we constructed an RNS model line which allows variable  $m_{1/2}$  while maintaining low electroweak naturalness  $\Delta_{EW} \sim 10 - 20$  and  $m_h \simeq 125$  GeV. We found that  $\tilde{g}\tilde{g}$  production followed by cascade decays leads to the expected leptons+jets+ $E_T^{\text{miss}}$  events. These should allow values of  $m_{\tilde{g}}$  up to  $\sim 1.7$  TeV to be discovered by LHC14 with about 300 fb<sup>-1</sup> of integrated luminosity.

A qualitatively new signal, endemic to SUSY models with light higgsinos, arises mainly from wino pair production  $pp \rightarrow \tilde{W}_2 \tilde{Z}_4 \rightarrow (W^\pm \tilde{Z}_{1,2}) + (W^\pm \tilde{W}_1^\mp)$  which leads to same sign-diboson production accompanied by minimal jet activity. After cuts, the largest background comes from  $t\bar{t}W$  production. This channel seems to offer the best reach for RNS for higher integrated luminosity values  $> 100$  fb<sup>-1</sup>. The SSdB signal from wino pair production may be confirmed if the decays of  $\tilde{W}_2$  and  $\tilde{Z}_4$  yield a final state with  $WZ \rightarrow 3\ell + E_T^{\text{miss}}$  at high integrated luminosity. Interestingly, wino pair production also leads to observable  $4\ell + E_T^{\text{miss}}$  signals for  $m_{1/2} \lesssim 500$  GeV (up to  $\sim 650$  GeV at the high-luminosity LHC). We also explored signals in the soft  $3\ell$  channel arising from direct higgsino pair production  $pp \rightarrow \tilde{W}_1^\pm \tilde{Z}_2$ . This channel should be visible over the lower  $m_{1/2}$  range, which provide a large enough  $m_{\tilde{Z}_2} - m_{\tilde{Z}_1}$  mass gap such that one may avoid the  $2 \rightarrow 4$  process  $W^*Z^*/W^*\gamma^*$  which contains an obstructing virtual photon contribution at the lower portion of the  $m(\ell^+\ell^-)$  distribution. Detection will likely be possible via the analysis of the shape of the dimuon invariant mass distribution for  $e^\pm\mu^+\mu^-$  events where there should be a distortion due to an excess for  $m(\mu^+\mu^-) < m_{\tilde{Z}_2} - m_{\tilde{Z}_1}$ .

The final reach situation is summarized in Table 5, where the  $5\sigma$  reach in terms of  $m_{\tilde{g}}$  is given for various discovery channels and integrated luminosity values. While LHC14 can explore RNS up to  $m_{\tilde{g}} \sim 2$  TeV for 300 fb<sup>-1</sup>, a large swath of parameter space with  $m_{\tilde{g}} \sim 2 - 5$  TeV seemingly lies beyond LHC14 reach.

The grand picture is shown in Fig. 16 where we plot the  $\mu$  vs.  $m_{1/2}$  plane of the RNS model, taking the GUT-scale matter scalar mass parameter  $m_0 = 5$  TeV,  $\tan\beta = 15$ ,  $A_0 = -1.6m_0$  and  $m_A = 1$  TeV. The green-shaded region has thermal higgsino relic density  $\Omega_{\tilde{h}} h^2 < 0.12$ , which allows for contributions to the dark matter density from axions[56]. The reader may legitimately ask whether the non-observation of any signal in WIMP direct

detection experiments excludes portions of this region. In this connection we should keep in mind that deep in this green region— *i.e.* for large values of  $m_{1/2}$  where the LSP is higgsino-like— the WIMP *thermal* relic density is strongly suppressed and in fact the dark matter is expected to be comprised of just 5-10% Higgsino-like WIMPs along with the bulk comprising of axions, or something else, over much of parameter space[56]. In such a case, the local WIMP abundance is expected to be suppressed by a factor 10-15 from the usual assumption, thus allowing the RNS higgsinos to escape present bounds. Even with a depleted local abundance, ton-size noble liquid detectors should be able to test the entire RNS parameter space with  $\Delta_{EW} < 100$ [57]. The recent null WIMP search results from the LUX[58] and XENON100[59] experiments will likely exclude a small region along the edge of the green region where the thermal neutralino relic density saturates the observed cold dark matter density. We have not performed a quantitative study to delineate this region, in part because effects from the sector responsible for the non-thermal-neutralino component of the dark matter could significantly modify this analysis. The neutralino contribution to the cold dark matter could be increased from its thermal expectation due to late decay of heavy fields to neutralinos, or reduced if new heavy fields decay to SM particles, leading to entropy-dilution of neutralinos. In the latter case, axions or some other particles beyond the MSSM would have to make up the balance.

From Figure 16, it can be seen that LHC8 has explored  $m_{1/2} < 400$  GeV via search for  $\tilde{g}\tilde{g}$  production. The LHC14 reach with  $300 \text{ fb}^{-1}$  for  $\tilde{g}\tilde{g}$  and for same-sign dibosons extends to  $\sim 700 - 800$  GeV (corresponding to a reach to  $m_{\tilde{g}} \sim 1.8 - 2.1$  TeV). The contours of  $\Delta_{EW} = 30$  extend well beyond the LHC14 reach, to  $m_{1/2} \sim 1200$  GeV. We also show the reach of various  $e^+e^-$  collider energy options (ILC or TLEP) for  $\sqrt{s} = 250, 500$  and  $1000$  GeV via the reaction  $e^+e^- \rightarrow \tilde{W}_1^+ \tilde{W}_1^-$  [60]. We see that ILC with  $\sqrt{s} \sim 600$  GeV can probe the entire parameter space with  $\Delta_{EW} < 30$ , thus either discovering or ruling out the light higgsinos which are a necessary condition for SUSY naturalness. Thus, LHC14 plus ILC600 can make a complete search for RNS models which automatically accommodate electroweak naturalness along with  $m_h \simeq 125$  GeV. These collider signals should also be accompanied by direct and perhaps indirect dark matter signals from detections of relic higgsinos[57], which would likely make up only a portion of the entire dark matter abundance.

## Acknowledgments

We thank Baris Altunkaynak for pointing out an error in some total cross sections of Fig. 4, 5 in the initial version. AM would like to thank FTPI at the University of Minnesota for hospitality during final stages of the project. This work was supported in part by grants from the U.S. Department of Energy, by Suranaree University of Technology, and by the Higher Education Research Promotion and National Research University Project of Thailand, Office of the Higher Education Commission.

NUHM2:  $m_0=5$  TeV,  $\tan\beta=15$ ,  $A_0=-1.6m_0$ ,  $m_A=1$  TeV,  $m_t=173.2$  GeV

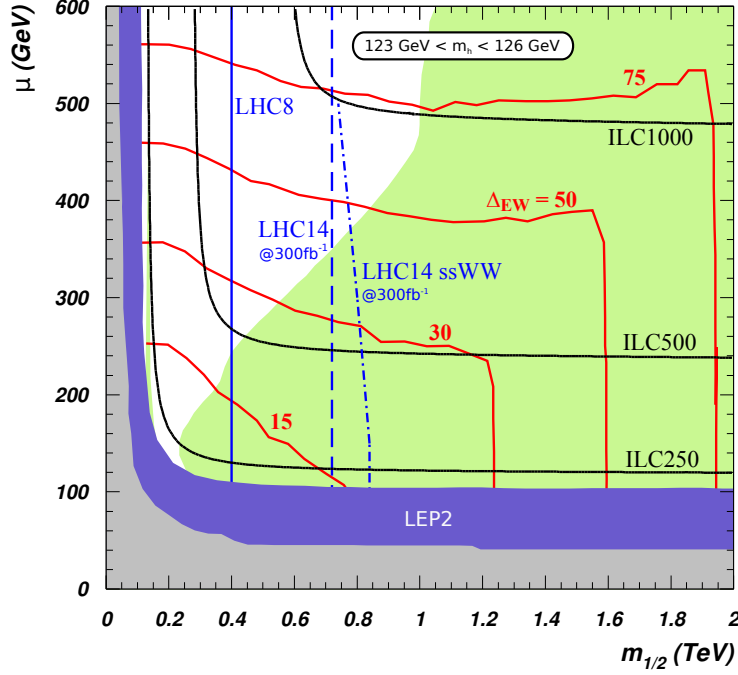


**Figure 16:** Plot of  $\Delta_{EW}$  contours (red) in the  $m_{1/2}$  vs.  $\mu$  plane of NUHM2 model for  $A_0 = -1.6m_0$  and  $m_0 = 5$  TeV and  $\tan\beta = 15$ . We also show the region accessible to LHC8 gluino pair searches (solid blue contour), and the region accessible to LHC14 searches with  $300 \text{ fb}^{-1}$  of integrated luminosity (dashed and dot-dashed contours). We also show the reach of various ILC machines for higgsino pair production (black contours). The green-shaded region has  $\Omega_{\tilde{Z}_1}^{std} h^2 < 0.12$ . The blue (gray) shaded region is excluded by LEP2 (LEP1) searches for chargino pair production. To aid the reader, we note that  $m_{\tilde{g}} \simeq 2.5m_{1/2}$ .

## References

- [1] G. Aad *et al.* [ATLAS Collaboration], *Phys. Lett. B* **716** (2012) 1 [arXiv:1207.7214 [hep-ex]].
- [2] S. Chatrchyan *et al.* [CMS Collaboration], *Phys. Lett. B* **716** (2012) 30 [arXiv:1207.7235 [hep-ex]].
- [3] G. Aad *et al.* [ATLAS Collaboration], *Phys. Rev. D* **87** (2013) 012008 [arXiv:1208.0949 [hep-ex]]; ATLAS-CONF-2013-04 and ATLAS-CONF-2013-061.
- [4] S. Chatrchyan *et al.* [CMS Collaboration], *J. High Energy Phys.* **1210** (2012) 018 [arXiv:1207.1798 [hep-ex]] and CMS-PAS-SUS-13-007.
- [5] A. Chamseddine, R. Arnowitt and P. Nath, *Phys. Rev. Lett.* **49** (1982) 970; R. Barbieri, S. Ferrara and C. Savoy, *Phys. Lett. B* **119** (1982) 343; N. Ohta, *Prog. Theor. Phys.* **70** (1983) 542; L. Hall, J. Lykken and S. Weinberg, *Phys. Rev. D* **27** (1983) 2359; CMSSM was introduced by G. Kane, C. Kolda, L. Roszkowski and J. Wells, *Phys. Rev. D* **49** (1994) 6173.
- [6] H. Baer, V. Barger and A. Mustafayev, *Phys. Rev. D* **87** (2013) 115028 [arXiv:1112.3017 [hep-ph]].

- [7] H. Baer, V. Barger, P. Huang, D. Mickelson, A. Mustafayev and X. Tata, *Phys. Rev. D* **87** (2013) 115028 [[arXiv:1212.2655](#) [hep-ph]].
- [8] R. Kitano and Y. Nomura, *Phys. Lett. B* **631** (2005) 58, *Phys. Rev. D* **73** (2006) 095004 and [hep-ph/0606134](#).
- [9] M. Papucci, J. T. Ruderman and A. Weiler, *J. High Energy Phys.* **1209** (2012) 035 [[arXiv:1110.6926](#) [hep-ph]].
- [10] N. Arkani-Hamed, talk at WG2 meeting, Oct. 31, 2012, CERN, Geneva.
- [11] H. Baer, V. Barger, P. Huang and X. Tata, *J. High Energy Phys.* **1205** (2012) 109 [[arXiv:1203.5539](#) [hep-ph]].
- [12] H. Baer, V. Barger, P. Huang, D. Mickelson, A. Mustafayev and X. Tata, *Phys. Rev. D* **87** (2013) 035017 [[arXiv:1210.3019](#) [hep-ph]].
- [13] H. Baer, V. Barger and D. Mickelson, [arXiv:1309.2984](#).
- [14] H. Baer, V. Barger, P. Huang, A. Mustafayev and X. Tata, *Phys. Rev. Lett.* **109** (2012) 161802.
- [15] C. Brust, A. Katz, S. Lawrence and R. Sundrum, *J. High Energy Phys.* **1203** (2012) 103 [[arXiv:1110.6670](#) [hep-ph]].
- [16] J. Ellis, K. Olive and Y. Santoso, *Phys. Lett. B* **539** (2002) 107; J. Ellis, T. Falk, K. Olive and Y. Santoso, *Nucl. Phys. B* **652** (2003) 259; H. Baer, A. Mustafayev, S. Profumo, A. Belyaev and X. Tata, *Phys. Rev. D* **71** (2005) 095008 and *J. High Energy Phys.* **0507** (2005) 065, and references therein.
- [17] H. Baer, V. Barger, P. Huang, D. Mickelson, A. Mustafayev, W. Sreethawong and X. Tata, *Phys. Rev. Lett.* **110** (2013) 151801.
- [18] H. Baer, V. Barger, G. Shaughnessy, H. Summy and L. -t. Wang, *Phys. Rev. D* **75** (2007) 095010.
- [19] R. Kadala, [arXiv:1205.1267](#).
- [20] ISAJET, by H. Baer, F. Paige, S. Protopopescu and X. Tata, [hep-ph/0312045](#).
- [21] H. Baer, C. H. Chen, R. Munroe, F. Paige and X. Tata, *Phys. Rev. D* **51** (1995) 1046; H. Baer, J. Ferrandis, S. Kraml and W. Porod, *Phys. Rev. D* **73** (2006) 015010.
- [22] S. Martin and M. Vaughn, *Phys. Rev. D* **50** (1994) 2282; V. D. Barger, M. S. Berger and P. Ohmann, *Phys. Rev. D* **47** (1993) 1093.
- [23] H. Haber and R. Hempfling, *Phys. Rev. D* **48** (1993) 4280.
- [24] D. Pierce, J. Bagger, K. Matchev and R. Zhang, *Nucl. Phys. B* **491** (1997) 3.
- [25] W. Beenakker, R. Hopker and M. Spira, [hep-ph/9611232](#).
- [26] R. Kadala, P. Mercadante, K. Mizukoshi and X. Tata, *Eur. Phys. J. C* **56** (2008) 511.
- [27] ATLAS Collaboration, [arXiv:1307.7292](#) [hep-ex]
- [28] J. Olsen, Talk presented at Snowmass Energy Frontier Workshop, Seattle (July, 2013).
- [29] For recent work, see *e.g.* C. Han, A. Kobakhidze, N. Liu, A. Saavedra, L. Wu and J. M. Yang, [arXiv:1310.4274](#).

- [30] H. Baer, X. Tata and J. Woodside, *Phys. Rev. D* **42** (1990) 1568.
- [31] H. Baer, C.-h. Chen, M. Drees, F. Paige and X. Tata, *Phys. Rev. D* **58** (1998) 075008.
- [32] T. Han, S. Padhi and S. Su, [arXiv:1309.5966](#) [hep-ph].
- [33] H. Baer, J. Ellis, G. Gelmini, D. Nanopoulos and X. Tata, *Phys. Lett. B* **161** (1985) 175; G. Gamberini, *Z. Physik C* **30** (1986) 605; H. Baer, V. Barger, D. Karatas and X. Tata, *Phys. Rev. D* **36** (1987) 96.
- [34] I. Hinchliffe, F. E. Paige, M. D. Shapiro, J. Soderqvist and W. Yao, *Phys. Rev. D* **55** (1997) 5520.
- [35] See J. Gaunt, C-H. Kom, A. Kulesza and W. J. Stirling, *Eur. Phys. J. C* **69** (2010) 53, for a recent assessment of dileptons from  $SS W$  production and other SM sources at the LHC.
- [36] M. L. Mangano, M. Moretti, F. Piccinini, R. Pittau and A. D. Polosa, *J. High Energy Phys.* **0307** (2003) 001.
- [37] J. Alwall, M. Herquet, F. Maltoni, O. Mattelaer and T. Stelzer, *J. High Energy Phys.* **1106** (2011) 128 [[arXiv:1106.0522](#) [hep-ph]].
- [38] T. Sjostrand, S. Mrenna and P. Z. Skands, *J. High Energy Phys.* **0605** (2006) 026.
- [39] J. Alwall, A. Ballestrero, P. Bartalini, S. Belov, E. Boos, A. Buckley, J. M. Butterworth and L. Dudko *et al.*, *Comput. Phys. Commun.* **176** (2007) 300.
- [40] J. M. Campbell and R. K. Ellis, *Nucl. Phys. Proc. Suppl.* **205-206**, 10 (2010) [[arXiv:1007.3492](#) [hep-ph]].
- [41] M. V. Garzelli, A. Kardos, C. G. Papadopoulos and Z. Trocsanyi, *J. High Energy Phys.* **1211** (2012) 056.
- [42] H. Baer, V. Barger, A. Lessa and X. Tata, *Phys. Rev. D* **86** (2012) 117701.
- [43] H. Baer, V. Barger, A. Lessa and X. Tata, *J. High Energy Phys.* **0909** (2009) 063.
- [44] S. Chatrchyan *et al.* [CMS Collaboration], *Phys. Rev. Lett.* **109** (2012) 071803 and [arXiv:1212.6194](#) [hep-ex]. See CMS-PAS-SUS-13-013 for an updated (preliminary) analysis.
- [45] [ATLAS Collaboration], ATLAS-CONF-2013-007
- [46] CMS Collaboration, CMS Physics Analysis Summary, CMS-PAS-SUSY-13-006 (2013).
- [47] D. Dicus, S. Nandi and X. Tata, *Phys. Lett. B* **129** (1983) 451; A. Chamseddine, P. Nath and R. Arnowitt, *Phys. Lett. B* **129** (1983) 445; H. Baer and X. Tata, *Phys. Lett. B* **155** (1985) 278; H. Baer, K. Hagiwara and X. Tata, *Phys. Rev. Lett.* **57** (1986) 294 and *Phys. Rev. D* **35** (1987) 1598; R. Arnowitt and P. Nath, *Mod. Phys. Lett. A* **2** (1987) 331; R. Barbieri, F. Caravaglios, M. Frigeni and M. Mangano, *Nucl. Phys. B* **367** (1991) 28; H. Baer and X. Tata, *Phys. Rev. D* **47** (1993) 2739; J. Lopez, D. Nanopoulos, X. Wang and A. Zichichi, *Phys. Rev. D* **48** (1993) 2062 and *Phys. Rev. D* **52** (1995) 142; H. Baer, C. Kao and X. Tata, *Phys. Rev. D* **48** (1993) 5175; S. Mrenna, G. Kane, G. Kribs and J. Wells, *Phys. Rev. D* **53** (1996) 1168; H. Baer, C. H. Chen, F. Paige and X. Tata, *Phys. Rev. D* **54** (1996) 5866; K. Matchev and D. Pierce, *Phys. Rev. D* **60** (1999) 075004; H. Baer, M. Drees, F. Paige, P. Quintana and X. Tata, *Phys. Rev. D* **61** (2000) 095007; V. Barger, C. Kao and T. Li, *Phys. Lett. B* **433** (1998) 328; V. Barger and C. Kao, *Phys. Rev. D* **60** (1999) 115015; K. Matchev and D. Pierce, *Phys. Lett. B* **467** (1999) 225; H. Baer, T. Krupovnickas and X. Tata, *J. High Energy Phys.* **0307** (2003) 020.



- [48] H. Baer, V. Barger, S. Kraml, A. Lessa, W. Sreethawong and X. Tata, *J. High Energy Phys.* **1203** (2012) 092 [[arXiv:1201.5382 \[hep-ph\]](#)].
- [49] Talks presented by C. Potter (for ATLAS Collaboration) and B. Hooberman (for CMS collaboration) at SUSY 2013, *21<sup>st</sup> International Conference on Supersymmetry and Unification of Fundamental Interactions*, Trieste, Italy, Aug. 2013.
- [50] M. L. Mangano, M. Moretti, F. Piccinini and M. Treccani, *J. High Energy Phys.* **0701** (2007) 013 [[hep-ph/0611129](#)].
- [51] [ATLAS Collaboration], ATLAS-CONF-2013-036.
- [52] The CMS Collaboration, CMS-PAS-SUS-13-010
- [53] H. Baer, T. Krupovnickas, S. Profumo and P. Ullio, *J. High Energy Phys.* **0510** (2005) 020.
- [54] H. Baer, M. Drees, F. Paige, P. Quintana and X. Tata, *Phys. Rev. D* **61** (2000) 095007.
- [55] H. Baer, V. Barger and P. Huang, *J. High Energy Phys.* **1111** (2011) 031.
- [56] K.-Y. Choi, J. E. Kim, H. M. Lee and O. Seto, *Phys. Rev. D* **77** (2008) 123501; H. Baer, A. Lessa, S. Rajagopalan and W. Sreethawong, *JCAP***1106** (2011) 031; H. Baer, A. Lessa and W. Sreethawong, *JCAP***1201** (2012) 036; K. J. Bae, H. Baer and A. Lessa, *JCAP* **1304** (2013) 041; K. J. Bae, H. Baer and E. J. Chun, [arXiv:1309.0519 \[hep-ph\]](#) and [arXiv:1309.5365 \[hep-ph\]](#).
- [57] H. Baer, V. Barger and D. Mickelson, [arXiv:1303.3816 \[hep-ph\]](#); H. Baer, V. Barger, D. Mickelson and X. Tata, [arXiv:1306.4183 \[hep-ph\]](#).
- [58] LUX Collaboration, D. Akerib *et al.* [arXiv:1310.8214 \[astro-ph\]](#).
- [59] XENON100 Collaboration, E. Aprile *et al.* *Phys. Rev. Lett.* **109** (2012) 181301.
- [60] M. Berggren, F. Brümmer, J. List, G. Moortgat-Pick, T. Robens, K. Rolbiecki and H. Sert, [arXiv:1307.3566 \[hep-ph\]](#).